

# **Surface Finish Optimization in Electrical Discharge Machining**

**Alberto Gonçalves do Poço**

Thesis to obtain the Master of Science Degree in

**Mechanical Engineering**

Supervisors: Prof. Pedro Alexandre Rodrigues Carvalho Rosa

Prof. José Duarte Ribeiro Marafona

## **Examination Committee**

Chairperson: Prof. Rui Manuel dos Santos Oliveira Baptista

Supervisor: Prof. Pedro Alexandre Rodrigues Carvalho Rosa

Members of the Committee: Prof. José Firmino Aguilár Madeira

Eng. Afonso José de Vilhena Leitão Gregório

**June 2018**



# Resumo

O processo de eletroerosão tem um importante papel no sector dos moldes, cunhos e cortantes, e na indústria em geral, complementando as tecnologias convencionais no fabrico de componentes metálicos de precisão. A presente investigação procura identificar os parâmetros operativos que controlam o acabamento superficial e determinar qual a combinação destes parâmetros que permite minimizar a rugosidade das superfícies maquinadas. Esta investigação experimental tem por base a maquinagem do AA1050 A com eléctrodo-ferramenta em cobre eletrolítico em regime de acabamento. Os principais parâmetros operativos em análise foram a corrente e tempo de pulso. Os resultados mostram que a rugosidade superficial diminui com a energia de descarga, associada à redução simultânea da corrente e tempo da descarga. Adicionalmente, a rugosidade do eléctrodo-ferramenta mostra também influenciar a rugosidade da superfície maquinada na peça.

**Palavras-Chave:** Eletroerosão, Otimização, Rugosidade, Influência da Rugosidade do Eléctrodo.

# Abstract

Electrical Discharge Machining plays an important role in the sector of molds, dies and cutters, and in the industry overall, being a complement to conventional technologies in the manufacture of precision metallic components. The current research seeks to identify the operating parameters that control the surface finish and establish which should be the combination of parameters that allows to minimize the roughness of the machined surfaces. This experimental research is based on the machining of AA1050 A with electrolytic copper tool-electrode in finishing operations. The main operative parameters in question were the current and pulse on time. The results show that the superficial roughness declined with the discharge energy, associated with the current simultaneous reduction and the discharge time. In addition, the electrode roughness also shows influence on the machined surface roughness.

**Keywords:** Electrical Discharge Machining, Optimization, Surface Roughness, Electrode Roughness Influence.

# Acknowledgements

Neste espaço pretendo prestar os meus sinceros agradecimentos às pessoas que me ajudaram ao longo deste percurso, pela partilha de conhecimentos e amizade.

Em primeiro lugar agradeço ao meu orientador, Professor Pedro Rosa, pela excelente orientação, motivação e conhecimento transmitido. Um agradecimento também ao Professor José Marafona, coorientador desta tese pelos conhecimentos transmitidos.

À equipa do NOF, por todos os esclarecimentos que dizem respeito à componente técnica da tese, e a amizade desenvolvida nestes meses de trabalho.

À minha família e à Verónica, por toda e qualquer razão.

# Contents

- Resumo ..... III
- Abstract ..... IV
- Acknowledgements ..... V
- Contents ..... VI
- List of Figures ..... VII
- List of Tables ..... X
- Abbreviations ..... XI
- List of Symbols ..... XII
- 1 Introduction ..... 1
- 2 Electrical Discharge Machining ..... 2
  - 2.1 Technical Variants and Industrial Applications ..... 3
  - 2.2 Process Parameters ..... 4
  - 2.3 Process Responses ..... 6
    - 2.3.1 Material Removal Rate ..... 6
    - 2.3.2 Electrode Wear Rate ..... 7
    - 2.3.3 Surface Condition ..... 9
    - 2.3.4 Process Responses Optimization ..... 11
- 3 Experimental Development ..... 14
  - 3.1 Measuring Instruments ..... 15
  - 3.2 Experimental Apparatus ..... 17
  - 3.3 Experimental Plan ..... 19
- 4 Results ..... 20
  - 4.1 Electrical Parameters Influence ..... 20
  - 4.2 Electrode Roughness Influence ..... 28
    - 4.2.1 Workpiece Roughness Evolution ..... 29
    - 4.2.2 Electrode Roughness Evolution ..... 35
  - 4.3 Optimization & Technological Approach ..... 39
- 5 Conclusions and future work ..... 44
- Bibliography ..... 45

# List of Figures

Figure 2-1 - (a) Working principle of EDM [4]; (b) Surface layers after electrical discharge machining [3]; (c) EDM different stages.....	2
Figure 2-2 - EDM typical elements. (a) Die-Sinker EDM elements and (b) Wire EDM elements [2]. ....	3
Figure 2-3 – (a) Die-sinker EDM machine, (b) Wire EDM machine, (c) Drilling EDM machine, (d) Die-Sinking EDM part [5], (e) Wire EDM part, (d) Drilling EDM standard.....	3
Figure 2-4 - (a) Gap voltage and current waveform [2]; (b) Actual profile of single EDM pulse [3]. ....	4
Figure 2-5 – (a) Material removal rate behaviour when subjected to different levels of dielectric pressure and peak current; (b) Surface roughness when subjected to different levels of dielectric pressure and peak current; (c) Material removal rate behaviour when subjected to different levels of tool diameter and peak current; Tool wear rate behaviour when subjected to different levels of tool diameter and peak current [10]. ....	6
Figure 2-6 – (a) Influence of the heat source parameters on material removal rate [11] and (b) Relationship between the MRR and EDM parameters [12]. ....	7
Figure 2-7 - Electrode wear in x and y directions [13]. ....	7
Figure 2-8 - Relationship of current with electrode wear; (a) along the width, (b) along the length [13].	8
Figure 2-9 - Relationship of current with wear ration ( $V=10$ ) [13]. ....	9
Figure 2-10 - Relationship between the average white layer and EDM parameters [12]. ....	9
Figure 2-11 - Several profiles presented on a machined surface. ....	10
Figure 2-12 - (a) Arithmetical mean roughness; (b) Mean roughness depth. ....	10
Figure 2-13 - (a) Variation of $R_a$ with discharge current for various hard steels using Cu electrodes [15]; (b) Relationship between the surface roughness and EDM parameters [12]. ....	10
Figure 2-14 - Task Manager on EDM optimization study (adapted from [4]). ....	12
Figure 3-1 – (a) Die-Sinker EDM Act Spark SP1; (b) Electrode and workpiece in their fixtures; (c) Proof Body.....	15
Figure 3-2 - Electrical measuring instruments. (a) Voltage differential probe, Hameg 100 Hz; (b) Current transformer CT-0.5; (c) Digital oscilloscope agilent 1000. ....	16
Figure 3-3 - Electrical measuring instruments verification sketch. (a) Oscilloscope verification; (b) Voltage differential probe verification; (c) Current probe verification. ....	16
Figure 3-4 - Measuring instruments of geometry and mass. (a) surface roughness measuring instrument; (b) Weight balance; (c) Microscope. ....	16
Figure 3-5 - Geometry standards. (a) Surface roughness standard; (b) Microscope standard. ....	17
Figure 3-6 - (a) Schematical apparatus; (b) Experimental apparatus. ....	17
Figure 3-7 - Typical EDM electrical signature acquired on experiments.....	18
Figure 3-8 - (a) Machined workpiece surface and (b) its respective electrical signature. ....	18
Figure 4-1 - Relationship between $R_aW$ and electrical parameters, for an open voltage of 80 V and pulse off time of 3 $\mu$ s. ....	23
Figure 4-2 - Relationship between $R_zW$ and electrical parameters, for an open voltage of 80 V and pulse off time of 3 $\mu$ s. ....	23

Figure 4-3 - Relationship between $RaW$ and $RaW$ .....	24
Figure 4-4 - Relationship between $RaEf$ and electrical parameters, for an open voltage of 80 V and pulse off time of 3 $\mu$ s. ....	24
Figure 4-5 - Relationship between $RzEf$ and electrical parameters, for an open voltage of 80 V and pulse off time of 3 $\mu$ s. ....	25
Figure 4-6 – Relationship between $RzEf$ and $RaEf$ . ....	25
Figure 4-7 - Relationship between MRR and electrical parameters, for an open voltage of 80 V and pulse off time of 3 $\mu$ s. ....	26
Figure 4-8 - Relationship between EWR and electrical parameters, for an open voltage of 80 V and pulse off Time of 3 $\mu$ s. ....	26
Figure 4-9 - Relationship between WR and electrical parameters, for an open voltage of 80 V and pulse off time of 3 $\mu$ s. ....	27
Figure 4-10 – (a) & (b) S/N plot and (c) & (d) Data means for WR. ....	28
Figure 4-11 – Proof body after machining for an experiment of 90 minutes with a rough electrode. (a) Electrode after machining; (b) Workpiece machined surface.....	30
Figure 4-12 - Electrode surface roughness influence on workpiece machined surface.....	31
Figure 4-13 - Electrode roughness influence. ....	32
Figure 4-14 - Plot of influence constants vs initial electrode average surface roughness. ....	33
Figure 4-15 - Workpiece surface roughness evolution.....	34
Figure 4-16 - Workpiece roughness evolution.....	35
Figure 4-17 - Electrode surface roughness evolution. ....	35
Figure 4-18 - Electrode surface roughness evolution. ....	36
Figure 4-19 - Electrode roughness evolution. (a) 30 minutes, (b) 60 minutes, (c) 90 minutes. ....	37
Figure 4-20 - Electrode surface roughness evolution. ....	38
Figure 4-21 - Workpiece surface roughness evolution plotted with model equation. ....	39
Figure 4-22 - Electrode surface roughness evolution plotted with model equation. ....	39
Figure 4-23 - Optimization experiment. (a) Workpiece machined surface and (b) Electrode machined surface.....	40
Figure 4-24 – Optimization experiment digitalized surfaces. (a) Workpiece machined surface and (b) Electrode machined surface. Note, scale global dimension equal to 0.25 mm.....	40
Figure 4-25 - Proof body surface roughness plot for open voltage of 80 V, pulse off time of 3 $\mu$ s and pulse on time of 1 $\mu$ s. (a) $RaW$ relationship with electrical parameters; (b) $RzW$ relationship with electrical parameters; (c) $RaEf$ relationship with electrical parameters; (d) $RzEf$ relationship with electrical parameters. ....	41
Figure 4-26 - Proof body aesthetics for the multiple electrical signatures experiment. (a) Workpiece machined surface and (b) Electrode machined surface.....	42
Figure 4-27 - Proof body microscopic view for the multiple electrical signature experiments. (a) Workpiece machined surface and (b) Electrode machined surface. Note, global scale dimension equal to 0.25 mm.....	43



Figure 4-28 - Microscopic view of machined surfaces. (a) Workpiece machined surface for single electrical signature; (b) Workpiece machined surface for multiple electrical signatures. Note, global scale dimension equal to 0.1 mm..... 43

# List of Tables

- Table 1 - Design of Experiments based on a L9 orthogonal array..... 11
- Table 2 - Experimental Plan Sketch. .... 13
- Table 3 - AA 1050 chemical composition. .... 14
- Table 4 - Physical properties and Erosion Index of the Proof Body..... 14
- Table 5 - Castrol Ilocut EDM 200 typical characteristics..... 15
- Table 6 - Electrical parameters influence experimental plan. .... 19
- Table 7 - Electrode Roughness Influence experimental plan..... 19
- Table 8 - Electrical parameters experiments results. .... 20
- Table 9 - Workpiece microscopic view for the different electrical parameters. Note, real width dimension equal to 0.25 mm..... 21
- Table 10 - Workpiece aesthetics for the different electrical parameters. .... 21
- Table 11 - Electrode microscopic view for the different electrical parameters. Note, real width dimension equal to 0.25 mm..... 22
- Table 12 - Electrodes surface after machining for the different electrode parameters. .... 22
- Table 13 - Electrode Roughness Influence Experimental Plan and respective data. .... 29
- Table 14 - Workpieces machined during electrode influence experiments..... 30
- Table 15 - Electrodes used during electrode influence experiments. .... 31
- Table 16 – Workpieces and electrodes for experiments of 240 minutes. .... 33
- Table 17 - Experiments for a polished and a rougher workpiece as initial condition with polished electrodes. .... 34
- Table 18 - Process Responses data for Optimization Experiment. .... 40
- Table 19 - Program data..... 42
- Table 20 - Process Responses data for multiple electrical signatures. .... 42

# Abbreviations

EDM – Electrical Discharge Machining.

EWR – Electrode wear rate.

MRR – Material removal rate.

Ra – Arithmetical mean roughness.

Rz - Mean roughness depth.

S/N – Signal to Noise Ratio.

SR – Surface roughness.

WR – Wear ratio.

DOE – Design of experiments

# List of Symbols

$\alpha$  – cyclic relationship

$C_m$  – erosion resistance index

$C_p$  – specific heat

$\lambda$  – thermal conductivity

$I_e$  – discharge current

$\rho$  - density

$Ra_{Ei}$  – initial electrode arithmetical mean roughness

$Ra_{Ef}$  – final electrode arithmetical mean roughness

$Ra_W$  – workpiece arithmetical mean roughness

$Ra_{Wi}$  – initial workpiece arithmetical mean roughness

$Rz_{Ei}$  – initial electrode mean roughness depth

$Rz_{Ef}$  – final electrode mean roughness depth

$Rz_W$  – workpiece mean roughness depth

$t_e$  – discharge duration

$T_{on}$  – pulse on time

$T_{off}$  – pulse off time

$T_{mach}$  – machining time

$T_m$  – melting point

$U_o$  – open voltage

$U_e$  – discharge voltage

$W_e$  – discharge energy

# 1 Introduction

Electrical Discharge Machining is a non-conventional manufacturing process with absent mechanical contact between tool and workpiece, making it an ideal approach for machining cavities with high aspect ratio (slenderness) on workpieces of relative high hardness materials. With a high field of applications such as transport sector, mould making industry, and medical prostheses, this technology allows machining any electrical conductive material. Currently, in industrial environment this process is based on technological tables, helping operators on their tasks, in which they are used to determine the machining parameters. These empirical tables are indispensable, once there is no consolidated theory in terms of material removal rate or surface roughness. This thesis intends to evaluate the EDM performance in surface finish, where experiments were performed with AA 1050 A, using electrolytic copper electrodes, as an industrial reference.

This work gives special attention to discharge current and pulse on time influence on surface roughness, since these are the most important parameters of the heat source that controls the EDM process. Experimental plan concerning electrical parameters influence is based on a total of 9 experiments for constant depth. Results presented, show that the finest surface roughness is obtained minimizing discharge energy. Based on this conclusion, machined workpiece surface was minimized to a value of  $0.612 \mu\text{m}$  by setting the levels of discharge current ( $I_e$ ) to 0.8 A and pulse on time ( $T_{on}$ ) to 1  $\mu\text{s}$ , despite the significant machining time (around 9.5 hours) and a black dot standard ingrained on the workpiece and electrode surfaces.

Since Die-Sinking EDM, is a “copy” process, where the inverted electrode geometry is gradually machined on a workpiece, other study was made looking to understand how electrode surface roughness can influence machined surface roughness. Experimental plan to this study basically consists in electrodes with different initial surface roughness achieved by abrasive paper of different granulometries, combined for different machining times. Workpiece surface roughness significantly vary for different initial electrode surface roughness tending to stabilize after a certain machining time. Electrode roughness evolution presents a typical convergence behaviour where rougher electrodes tend to decay their roughness while the most polished to increase, tending both for a constant value.

At last, a machining strategy was planned to improve surface quality and reduce machining time, with different electrical signatures, that gradually decreases the discharge energy while increasing machining depth. The last machining is performed for  $I_e$  of 0.8 A and  $T_{on}$  of 1  $\mu\text{s}$ , resulting on a SR of  $0.721 \mu\text{m}$ , with an operation total time of 20 minutes, reducing significantly the number of black dots, where these are only placed on a small region of the machined surface.

# 2 Electrical Discharge Machining

EDM is a thermoelectric process which removes material through the action of a plasma occurring in the gap between the tool-electrode and the workpiece, being these immersed in a dielectric fluid. This material removal mechanism is achieved by establishing a pulsed DC voltage in the gap between the tool and the workpiece (figure 2-1-a), creating an electrical field between these previous two attracting microparticles of relative conductivity contained in the dielectric fluid, in order to ionize the medium for the formation of the plasma channel (“mass” of free electrons and positively charged particles) [1]. Ionization lasts a certain period (figure 2-1-c), in order to store the necessary energy before discharge can occur, also known by ignition delay time, described to be the time needed to the dielectric breakdown, and generate the electron avalanche by the acceleration of the initial electrons [2]. A spark is then generated by the fast increase of temperature and pressure. The energy carried through the discharge melts a certain amount of material, that is severally related to the discharge energy level. This amount of material then vaporizes from the electrode and workpiece. During discharge a bubble composed of typical gaseous products derived from EDM process, enlarges outward the plasma channel. This is disrupted the moment pulse ends, cutting out the energy provided to the discharge, in order to flush molten material from electrode and workpiece’s surface out of the erosion zone. EDM typical part is described to be composed by several surface layers (figure 2-1-b). A first, placed at the top, with electrode and workpiece residues that were molten during the process, followed by a second layer, named recast or white layer that was altered in terms of metallurgical structure by the process, and the third is the Heated Affected Zone, resulted from the fast temperature increase and decrease [3].

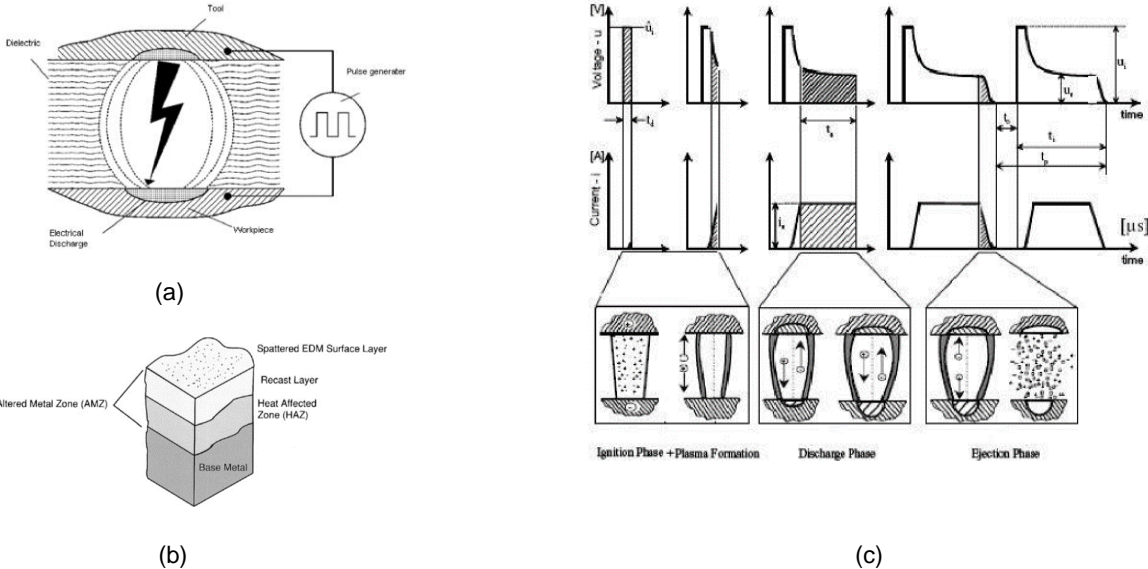


Figure 2-1 - (a) Working principle of EDM [4]; (b) Surface layers after electrical discharge machining [3]; (c) EDM different stages.

## 2.1 Technical Variants and Industrial Applications

Electrical Discharge Machining is usually the best alternative for products manufacturing unsuitable to be obtained by the conventional machining technology. EDM has several variants, for different geometry requirements. While Die-Sinking EDM is known for its ability of machining complex 3D cavities with high aspect ratio of high hardness electrical conductive materials, Wire EDM applies to 2D and 3D complex contours of parts with relative reduced thickness plates. These two variants typical elements are presented in figure 2-2.

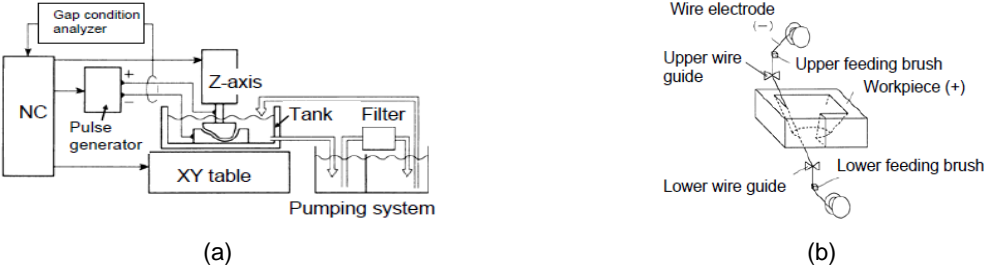


Figure 2-2 - EDM typical elements. (a) Die-Sinker EDM elements and (b) Wire EDM elements [2].

EDM also has a drilling variant to perform drills of small diameters, making this the best approach for drilling hard materials with a high depth, once there is no mechanical contact and material is removed by melting material from workpiece in process. Figures below, present these 3 general EDM variants and typical parts that can be manufactured by these technologies.



Figure 2-3 – (a) Die-sinker EDM machine, (b) Wire EDM machine, (c) Drilling EDM machine, (d) Die-Sinking EDM part [5], (e) Wire EDM part, (f) Drilling EDM standard.

## 2.2 Process Parameters

Process parameters are mainly of electric type, since the material removal mechanism heat input is based on a pulsed DC power supply with a certain waveform. Electrical parameters control consists in vary the voltage and current intensity and the pulse band width. Besides the electrical signature, there are several other non-electrical parameters that can significantly influence the erosive process, such of tool dimension, and dielectric pressure.

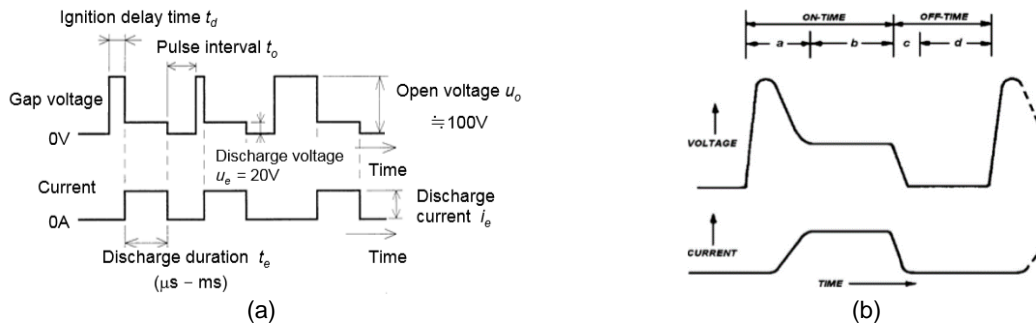


Figure 2-4 - (a) Gap voltage and current waveform [2]; (b) Actual profile of single EDM pulse [3].

As previously presented, EDM is a process thermoelectrically activated by establishing a pulsed DC voltage between electrode and part. Figure 2-4 (a) presents a theoretical electrical signature, based on gap voltage and current waveform that describe the EDM different stages and vary the parameters nomenclature. Open voltage ionizes the medium during a certain period storing the necessary energy to overcome the dielectric resistivity strength, called ignition delay time [2]. After dielectric breakdown, discharge occurs, where voltage falls to a lower value during discharge. This discharge voltage is uncontrollable for it depends on the electrode and workpiece materials and connecting interfaces, dielectric type, and normally lies between 10 and 40 V [6]. After discharge, pulse is disrupted, in a period called pulse interval,  $t_0$ . Current is flowing, since the dielectric breakdown until pulse is disrupted, being this period called discharge duration. Current Intensity is called discharge current. Summarizing all this different time periods, current and voltage terminologies that characterizes EDM waveforms, we obtain the main electrical parameters: open voltage, discharge voltage, discharge current, ignition delay time, discharge duration and pulse interval. Actual EDM waveforms are more similar to the one presented in figure 2-4-(b), where pulse on time is comprehended between the time voltage starts to rise and discharge current reaches its pre-set value by operator and starts falling. After this moment, until voltage restarts to rise is called pulse off time. Main electrical parameters used on optimization case studies are open voltage, discharge current, pulse on time and pulse off time. The combined voltage and current waveform deliver a certain energy level during pulse on time and a short time of deionization, depending on the dielectric characteristics. Energy carried through a discharge may be calculated by equation 1:

$$We = \int_0^{Ton} U(t).I(t)dt, \quad (1)$$



Where  $W_e$ , stands for the discharge energy [J];  $T_{on}$ , is the pulse duration [s];  $U(t)$ , is the voltage waveform [V] and  $I(t)$  the current waveform [A]. According to [7], the increase of these quantities increases material removal rate, while for achieving a better surface roughness these should decrease.

Besides electrical parameters there are other factors, with significant influence on the EDM process, such as the thermal properties of the materials being processed (specific heat, thermal conductivity and melting point), tool dimension, dielectric condition (pressure, flow rate, viscosity, ...). Material thermal properties play important role on EDM, since material is removed once it melts and vaporizes from gap region. The combined value of thermal conductivity, specific heat and melting temperature describe an erosion resistance index [8]. It can be calculated by equation 2:

$$Cm = \lambda C_p T_m^2 \quad (2)$$

where  $\lambda$  is the heat conductivity [ $W m^{-1} K^{-1}$ ],  $C_p$  is the specific heat [ $J m^{-3} K^{-1}$ ] and  $T_m$  is the melting point [K]. Workpiece material used, shall be of smaller index than materials used for the electrodes in order to have a reasonable relative wear between electrode and workpiece.

Dielectric fluid properties during the process, can significantly influence process responses, like surface roughness, material removal rate, etc. Dielectric fluids used on EDM are characterized by having a high dielectric strength and fast deionization the moment pulse ends [9]. Dielectric pressure has been used as project variable on EDM Optimization studies, together with electrical and non-electrical parameters. Figures 2-5 (a)-(d) are quote from a Balasubramanian's study concerning four project variables being these peak current, pulse on time, dielectric pressure and tool diameter. Balasubramanian concluded that material removal rate and tool wear rate are increased whenever dielectric pressure, peak current and dielectric pressure are increased. For surface roughness, optimum value is achieved by an intermediate value of peak current and dielectric pressure being least affected by tool diameter [10].

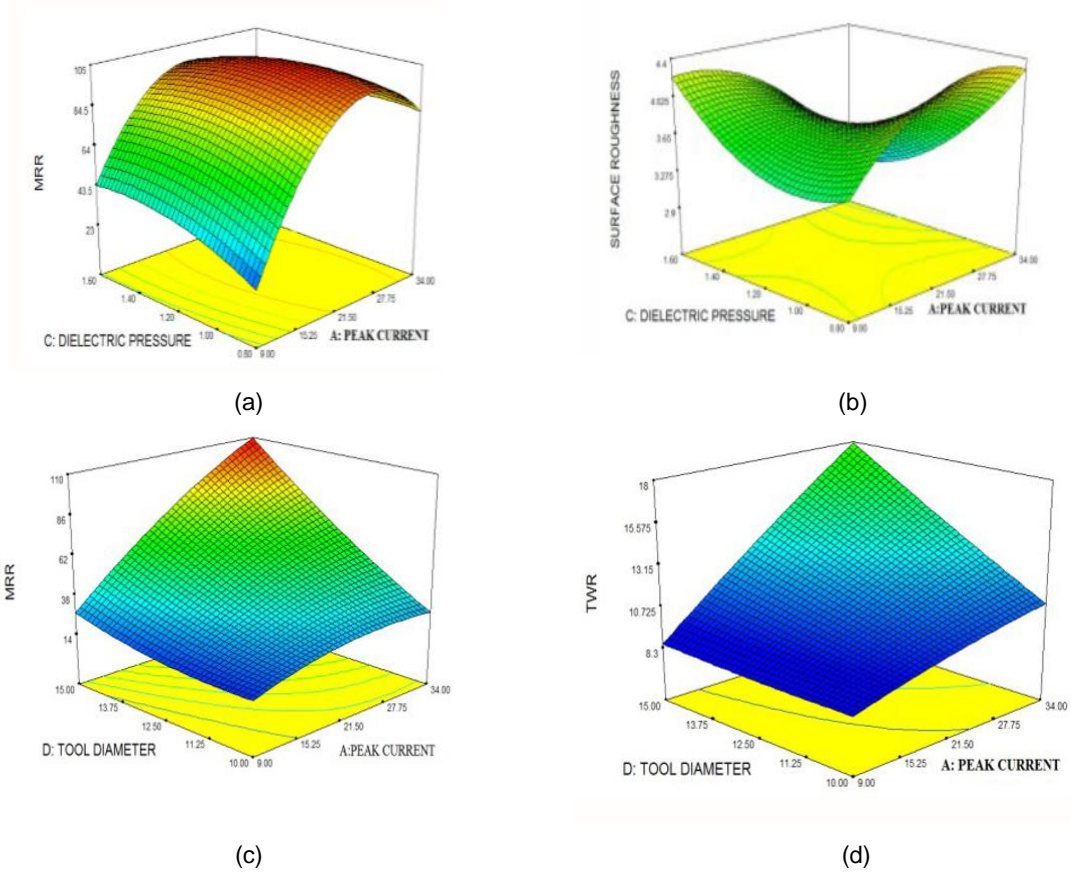


Figure 2-5 – (a) Material removal rate behaviour when subjected to different levels of dielectric pressure and peak current; (b) Surface roughness when subjected to different levels of dielectric pressure and peak current; (c) Material removal rate behaviour when subjected to different levels of tool diameter and peak current; Tool wear rate behaviour when subjected to different levels of tool diameter and peak current [10].

## 2.3 Process Responses

This document studies the influence of determined parameters that characterize the material removal mechanism by Electrical Discharge Machining on surface roughness. This work gives special attention to the workpiece surface roughness, but also to quantify material removal rate and electrode wear rate. This subchapter concerns the main process responses.

### 2.3.1 Material Removal Rate

Material removal rate expresses the material removed per unit of time. This factor is extremely important, because it defines a production rate or how fast we can process materials. This can be calculated by measuring initial and final weight of the workpiece and dividing its difference by machining time. The following mathematical expression is used to calculate MRR value:

$$MRR = \frac{Initial_{Weight} - Final_{Weight}}{Machining_{Time}} \left[ \frac{g}{min} \right] \quad (3)$$

$$MRR = \frac{Initial_{Volume} - Final_{Volume}}{Machining_{Time}} \left[ \frac{mm^3}{min} \right] \quad (4)$$

To quantify MRR, measuring the specimens weight, is more accurate, in order to avoid measuring errors, being this approach used on this study. MRR has been mostly studied related to discharge current and pulse on time, because these are which mainly influence this process response. Although electrical parameters have a relationship with discharge energy there is a tendency to evaluate each of them separately for  $I_e$  and  $t_e$ , because these have different effects on the process response. The following graphs presented in figure 2-6 concern the relationship between MRR and electrical parameters.

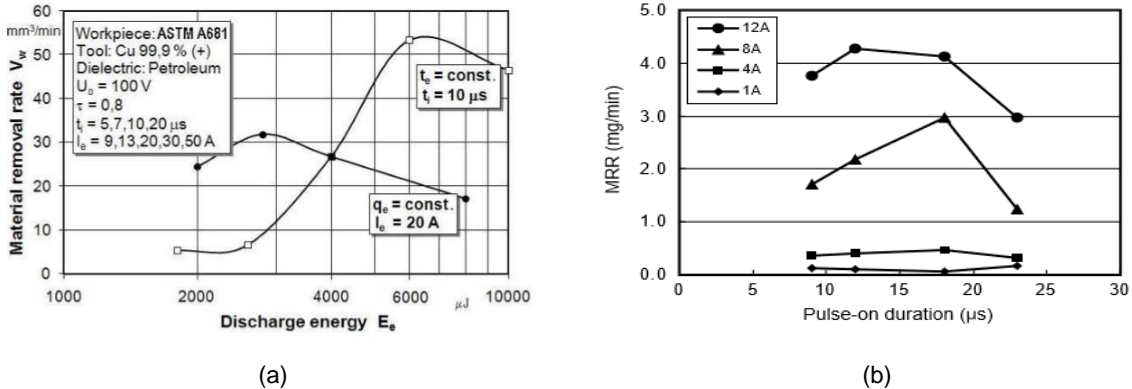


Figure 2-6 – (a) Influence of the heat source parameters on material removal rate [11] and (b) Relationship between the MRR and EDM parameters [12].

Figure 2-6 (a) deals with an influence study of  $W_e$  on MRR performed by [11], where he evaluates  $I_e$  and  $T_{on}$  separately, like the one presented by [12] in figure 2-6 (b). There is a general conclusion common to both, that for increasing  $I_e$  leads to higher MRR for a constant  $T_{on}$  ( $t_i$  in figure 2-6 (a)), where [12] that the gradual increase of  $T_{on}$  doesn't necessarily improve MRR. On the other hand, [11] refers that after  $I_e$  at 30 A (15 A/cm<sup>2</sup>), MRR starts to decrease due to the increase of discharge current is limited by the current density.

### 2.3.2 Electrode Wear Rate

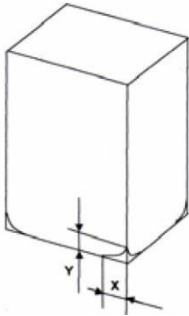


Figure 2-7 - Electrode wear in x and y directions [13].

Electrode Wear Rate expresses the electrode wear per unit of time. This can be calculated by measuring initial and final weight of the electrode and dividing its difference by machining time. EWR can be calculated by equations 5 and 6:

$$EWR = \frac{Initial_{Weight} - Final_{Weight}}{Machining\_Time} \left[ \frac{g}{min} \right] \quad (5)$$

$$EWR = \frac{Initial_{Volume} - Final_{Volume}}{Machining\_Time} \left[ \frac{mm^3}{min} \right] \quad (6)$$

Excessive electrode wear may cause unallowable defects, such as errors out of the dimensional tolerance range. A factor commonly used, is also the Wear Ratio or Relative Wear, that stands for the ratio between EWR and MRR. This concept is traduced in the percentage of material wasted on tool electrode for removing a certain quantity of material of a workpiece in process. Its mathematical expression is following presented:

$$WR = \frac{EWR}{MRR} \quad (7)$$

Where WR, stands for the wear ratio; EWR is the electrode wear rate [g/min]; and MRR stands for material removal rate [g/min]. Figure 2-8 is quote from a study performed by Khan, concerning discharge current influence on electrode wear rate.

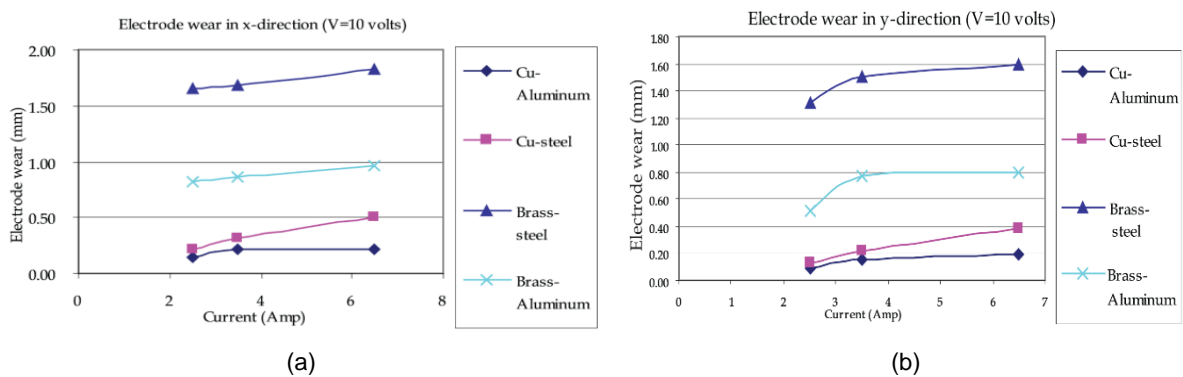


Figure 2-8 - Relationship of current with electrode wear; (a) along the width, (b) along the length [13].

Khan [13] considers not only the volumetric electrode wear but width and length dimensions where he denotes that it is not uniform in terms of width or length directions, being of higher value wear in width direction, due to the fact a smaller cross section allows a lower heat transfer than a larger cross section. His general conclusion about electrode wear rate is that it increases with discharge current. Furthermore, he accounts in his study WR, referring that is known that the current increase beside of the EWR decrease, induces MRR to increase. Figure 2-9 gathers his WR values where he concludes that the current increase leads WR to decrease.

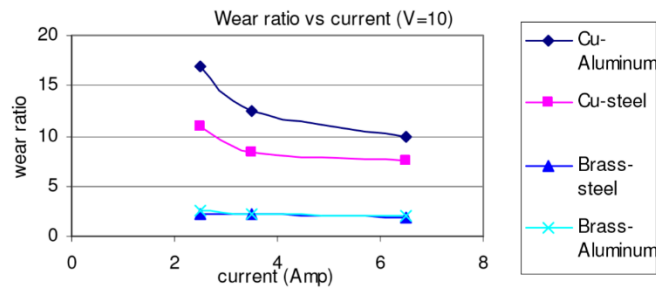


Figure 2-9 - Relationship of current with wear ration (V=10) [13].

### 2.3.3 Surface Condition

An important factor that also characterizes EDM performance is surface integrity. As presented before, in figure 2-1 (b), there are several layers that compose the surface machined by EDM. According to [14], this has three different surface layers, a first composed by molten and expelled material from both workpiece and electrode during the erosion process that spatter the surface, followed by the second layer, called white layer, where its metallurgical structure has been altered by violent temperature increase and decrease during the erosive process. Third and last layer is the heat affected zone, consequence of the EDM heating action. Lee [12] refers that predicting white layer thickness is a must, in order to avoid dimensional errors in the project phase. This is presented in the following figure 2-10, that contains the white layer thickness behaviour for different levels of  $I_e$  and  $T_{on}$ , where he concludes in a general way that its thickness increases for higher levels of  $I_e$  and  $T_{on}$  [12].

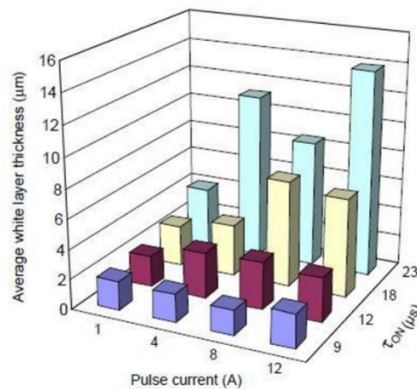


Figure 2-10 - Relationship between the average white layer and EDM parameters [12].

An important response to any manufacturing process is surface roughness that is a frequent project requirement and may appear in any technical drawing. Surface roughness is described to be the sum of irregularities that characterize a surface, due to the manufacturing process and errors of microgeometry, typical behavior of the surface of a certain material and can be defined in many different terms. A surface is composed for different profiles (figure 2-11). Roughness or primary texture is the set of irregularities caused by the manufacturing process, which are the impressions left by the tool (A), Secondary ripple or texture is the set of irregularities caused by vibrations or deflections of the production system or the heat treatment (B); Irregular orientation is the general direction of the texture components (C).

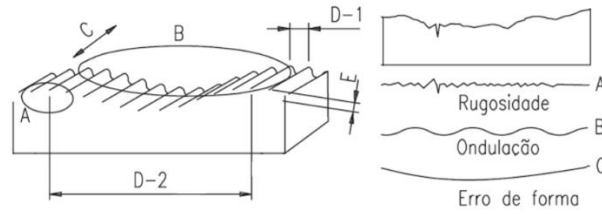


Figure 2-11 - Several profiles presented on a machined surface.

This study gives attention to the arithmetical mean roughness ( $R_a$ ), described by EN ISO 4287 to be the arithmetical mean of the absolute values of the profile deviations ( $y_i$ ) from the mean line of the roughness profile (Figure 2-12 (a)). It can be calculated by the following mathematical expression:

$$R_a = \frac{1}{l_m} \int_0^{l_m} |y(x)| dx \quad (8)$$

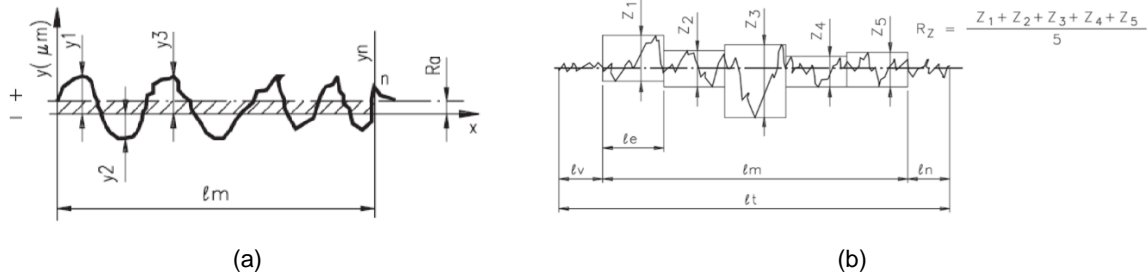


Figure 2-12 - (a) Arithmetical mean roughness; (b) Mean roughness depth.

Average distribution of vertical surface (mean roughness depth,  $R_z$ ) stands for the average of 5 distances measured from peak to valley in the measured length, illustrated in figure 2-12 (b). This is then an average of 5 peak to valley distances. Graphs presented in figure 2-13 consider two different studies. The first presented by [15], figure 2-13 (a), concerning  $R_a$  behaviour when subjected to different intensities of current. His results and conclusions are in conformity with [7]'s assumption above presented, and in a certain way with the second presented by [12], figure 2-13 (b), that surface roughness increases gradually with discharge current increase [15].

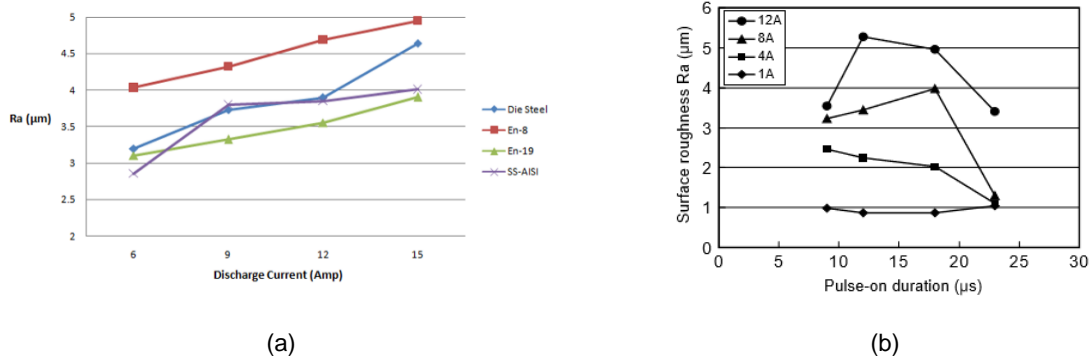


Figure 2-13 - (a) Variation of  $R_a$  with discharge current for various hard steels using Cu electrodes [15]; (b) Relationship between the surface roughness and EDM parameters [12].

Lee [12] concludes that SR increases with discharge current for a constant pulse-on duration. It may be observed in figure 2-13 (b) that for a certain  $T_{on}$ , roughness starts to decrease. This turning point is not common to every  $I_e$  series. The same happened for his results for MRR, where he refers this dramatic decrease is due to the expansion of plasma channel.

### 2.3.4 Process Responses Optimization

Electrical Discharge Machining has been one of the main target machining technologies used as optimization case study, since there is no consolidated theory in this material removal mechanism relating its waveform, electrical parameters and non-electrical parameters to the different process responses. Optimization studies are normally based on Taguchi Design of Experiments, where experiments number depend mainly on the project variables number as well for the levels of each variable. Experiments in Taguchi design are of smaller number, than the ones on traditional analysis where, for example, in a design with three variables with three operative levels, 9 experiments are enough for evaluate the design, and are based on a L9 orthogonal array.

Table 1 - Design of Experiments based on a L9 orthogonal array.

Exp N°	A	B	C
1	1	1	1
2	1	2	2
3	1	3	3
4	2	1	2
5	2	2	3
6	2	3	1
7	3	1	3
8	3	2	1
9	3	3	2

Table previously presented, sketches a DOE with 3 project variables, A, B and C, where each of them has 3 operative levels, 1, 2, 3. Taguchi analysis is then based on Signal-to-Noise ratio correlation functions, and Mean Data of each level, seeking the optimum parameter combination level for a certain process response. A proper task manager on optimization study is following presented, quote from Gaikwad EDM optimization study.

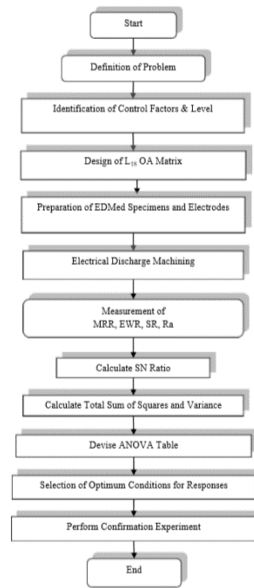


Figure 2-14 - Task Manager on EDM optimization study (adapted from [4]).

Optimum parameters combination levels shall be identified for the typical Taguchi signal-to-noise ratio equations, “smaller-the-better” in case we are looking for the combination that minimize a certain process response, following presented labelled with number (9), and “larger-the-better”, for the one that maximizes a certain objective function, labelled with number (10), where  $n$  is number of observations on a certain process response, and  $y$  is the response value. These equations are defined in a way that for both objectives larger S/N ratio value indicates our optimum result.

$$\frac{s}{N} = -10 \log_{10} \left( \frac{\sum_i^n (y_i^2)}{n} \right); \quad (9)$$

$$\frac{s}{N} = -10 \log_{10} \left( \frac{\sum_i^n (1/y_i^2)}{n} \right); \quad (10)$$

Mean Data is simply calculated as the average response of a certain level of a project variable. For example, looking to table 1, level 1 of variable A appears in the first 3 experiments. Thus, mean data response will be the sum of experiment n<sup>o</sup>1, 2 and 3, divided by three. Three main EDM process responses on optimization studies are MRR, EWR and SR, and obviously, there isn't an optimal parameter combination common to each of these, once maximum MRR is achieved for higher discharge energy levels that consequently lead to higher EWR, as well for a higher Ra because craters will be of higher depth and diameter. As explained before, optimal points are identified by S/N ratio and mean response data of each variable operative level, that generally result on a parameter combination level that was not covered up by the experimental plan. With this, we proceed to the field of confirmation tests. Based on mean response levels, results can be predicted in terms of the different EDM process responses. Predicted response value may be calculated by the following equation:



$$\alpha_{predicted} = \alpha_m + \sum_{i=1}^n (\alpha_0 - \alpha_m) \quad (11)$$

Where  $\alpha_{predicted}$  is the value of response at the resulted optimum parameter combination levels, to predict and validate the EDM process,  $\alpha_0$  is the mean data of a certain response at optimal parameter level of the factors, and  $\alpha_m$  is the average value of response and n is the number of factors [16]. Experimental plan on this work is a typical DOE of Taguchi Design, based on L9 orthogonal array with three levels and two factors. The same as in table 1, but with a absent third parameter, shown in table 2.

Table 2 - Experimental Plan Sketch.

Exp N°	A	B
1	1	1
2	1	2
3	1	3
4	2	1
5	2	2
6	2	3
7	3	1
8	3	2
9	3	3

This approach was chosen, in order to avoid some erroneous conclusions and clearly evaluate discharge current and pulse on time influence on the typical EDM process responses.

### 3 Experimental Development

The present work studies the material pair of electrolytic copper and aluminium alloy 1050 A machinability in finishing operations. This is a typical material choice, aluminium for its relative low density and price, and electrolytic copper due to its electrical and thermal conductivity, being a preferable electrode material for a case study. This proof body was processed in Mechanical Technology Laboratory, in a total of 35 electrodes and 35 workpieces. Dimensions chosen for electrodes geometry were  $30 \times 30 \times 5 \text{ mm}^3$ , and  $25 \times 25 \times 20 \text{ mm}^3$  for aluminium workpieces. Following table contains Aluminium 1050 A chemical composition.

Table 3 - AA1050 A chemical composition.

(%)	Si	Fe	Cu	Mn	Mg	Zn	Ti	Al	V	Others
AA	0.25	0.40	0.05	0.05	0.05	0.07	0.05	99.5	-	0.03
1050A	max	max	max	max	max	max	max	min		
EAA										

As presented in process parameters section, material thermal properties play a role as non-electrical parameters, where Reynaerts defines an Erosion Resistance Index. Properties that compose Erosion Index are Specific Heat, Thermal Conductivity and Melting Point. Table 4 presents the proof body's physical properties and respective erosion index.

Table 4 - Physical properties and Erosion Index of the Proof Body.

Properties/Materials	AA1050 A	Copper
Melting point [K]	923	1356
Specific Heat [J/(kg.K)]	900	381
Thermal Conductivity [W/(m.K)]	231	392
Density [Kg/m <sup>3</sup> ]	2700	8910
Index Cm [J <sup>2</sup> /(m.s.kg)]	1.771E+11	2.75E+11

As Reynaerts presents, a high Cm leads us to a fine electrode material, and a low Cm to a fine workpiece material. Looking at the previews table, we denote that aluminium has a lower Cm than copper. Aluminium has a high Thermal Conductivity and Specific Heat, making difficult a fast temperature increase, on the other hand, Aluminium melting point is around 650 °C, lower than other workpieces like Steel. Dielectric Fluid used for experiments was a Castrol Ilocut EDM 200 with typical characteristics presented in the following table.

Table 5 - Castrol Ilocut EDM 200 typical characteristics.

	Test Method	Units	Values
Density at 15 °C	ISO 3675, ASTM D1296	$kg/m^3$	765
Aesthetics	ISO 2049	-	transparent
Odour		-	odorless
Initial Inflammation Point	ISO 2719, ASTM D93	°C	104
Final Inflammation Point	ISO 2592, ASTM D92	°C	106
Kinematical Viscosity at 20 °C	ISO 3105, ASTM D446	$mm^2/s$	2.9
Neutralization Number	ASTM D974	mgKOH/g	0.01
Initial Boiling Point	ISO 3405, ASTM D86	°C	235
Final Boiling Point	ISO 3405, ASTM D86	°C	245
Aromatical Content	ASTM D 2140	%	<0.001

Experiments were performed on a CNC Die-Sinking Machine, ACT Spark SP1, presented in figure 3-1 (a), and consisted on an open pocket machining operation with an area of  $5 \times 20 \text{ mm}^2$ . As seen on figure 3-1 (c), electrode surface area is bigger than the machined workpiece surface, to have a suitable access for the surface roughness measurement, and different measuring lengths that are required depending on the SR value measured.

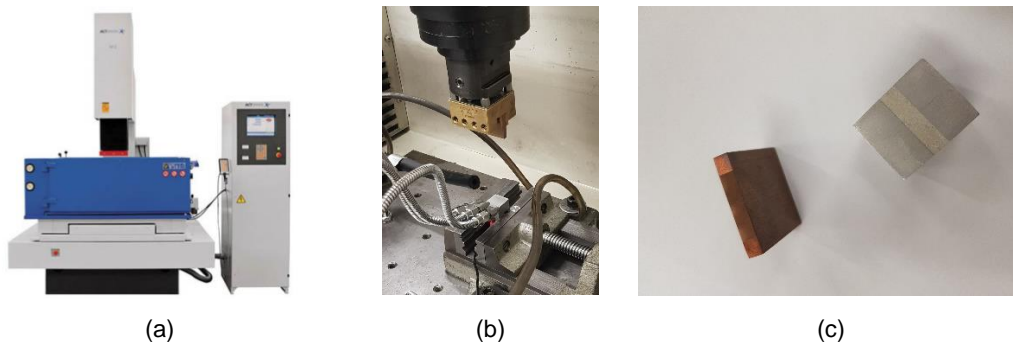


Figure 3-1 – (a) Die-Sinker EDM Act Spark SP1; (b) Electrode and workpiece in their fixtures; (c) Proof Body.

### 3.1 Measuring Instruments

A certain number of instruments were needed in order to create an experimental apparatus, since the electrical devices that are used to acquire the EDM electrical signature, to the other measuring instruments used to quantify material removal and surface roughness. Figures 3-2 (a)-(c) concern the electrical measuring instruments, being these the ones used during experiments.

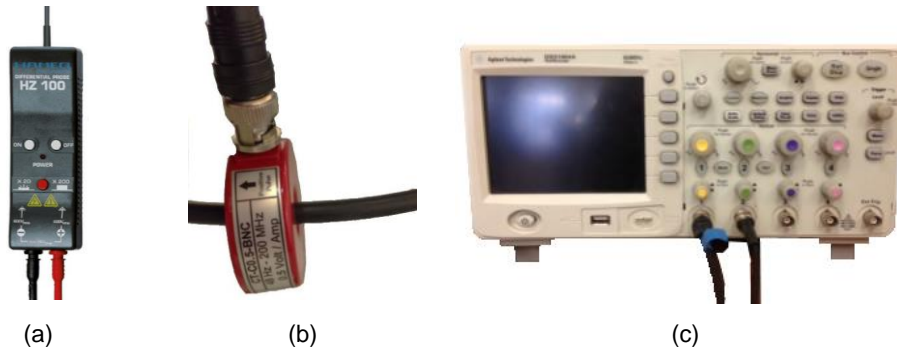


Figure 3-2 - Electrical measuring instruments. (a) Voltage differential probe, Hameg 100 Hz; (b) Current transformer CT-0.5; (c) Digital oscilloscope Agilent 1000.

Electrical measuring instruments above presented compose the experimental apparatus developed in the Die-Sinker EDM machine presented in figure 3-1 (a). Voltage differential probe, figure 3-2 (a), intends to acquire EDM voltage waveform, measured in the gap between electrode and workpiece having a 20x signal attenuation. Current probe above presented in figure 3-2 (b), is placed surrounding the power cable, working by Hall Effect principle, acquiring values in volts having a strict relation  $0.5 \text{ V/A}$  between reading and real values. This device is then used to acquire current waveform. These electrical waveforms are read on the digital oscilloscope seen in figure 3-2 (c). These instruments are carefully verified before the experiments in order to guarantee the correct values used on parameters, and to see if there is a need of calibration to any of them. Oscilloscope is first verified with a signal generator and then electrical probes with a power source and oscilloscope. Verification consists in comparing input and output values.

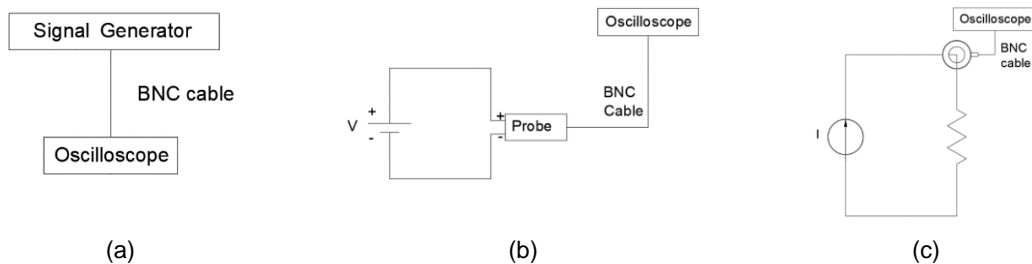


Figure 3-3 - Electrical measuring instruments verification sketch. (a) Oscilloscope verification; (b) Voltage differential probe verification; (c) Current probe verification.

Besides electrical measuring instruments type, others are used to measure physical quantities and with this, establish a relation between process parameters and process responses. These instruments are presented in figures 3-4 (a)-(c).

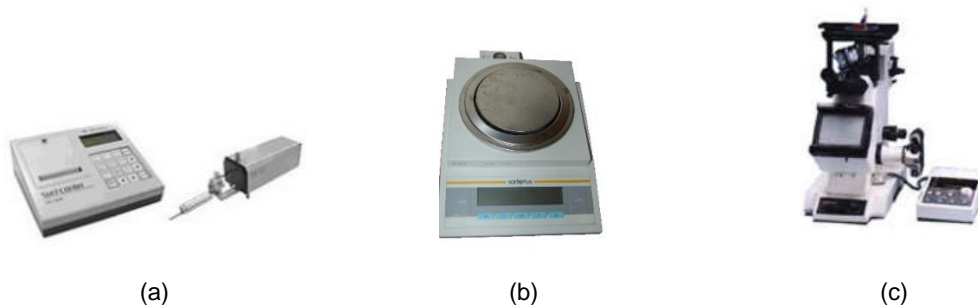


Figure 3-4 - Measuring instruments of geometry and mass. (a) surface roughness measuring instrument; (b) Weight balance; (c) Microscope.

Proof body weight is measured before and after experiments (figure 3-4 (b)) so that material removal rate and electrode wear rate may be quantified. This also applies to the Surface Roughness Measurement that is achieved by using the instrument presented in figure 3-4 (b). After experiments, surface is viewed and digitalized on the microscope (figure 3-4 (c)). As for the electrical measuring instruments, these instruments are verified, simply by measuring appropriated standards and comparing theoretical value and measured value.

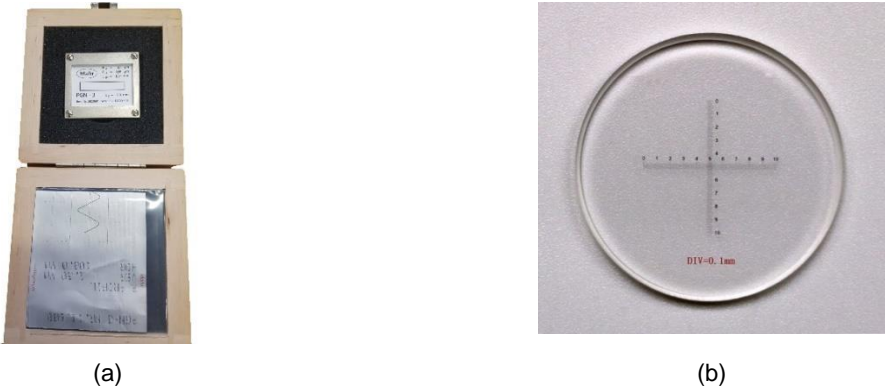


Figure 3-5 - Geometry standards. (a) Surface roughness standard; (b) Microscope standard.

Surface roughness measuring instrument was verified with a SR standard, resulting an allowable error around 0.011  $\mu\text{m}$ . Microscope calliper is used for scaling the measurement, being indispensable for all measurements.

### 3.2 Experimental Apparatus

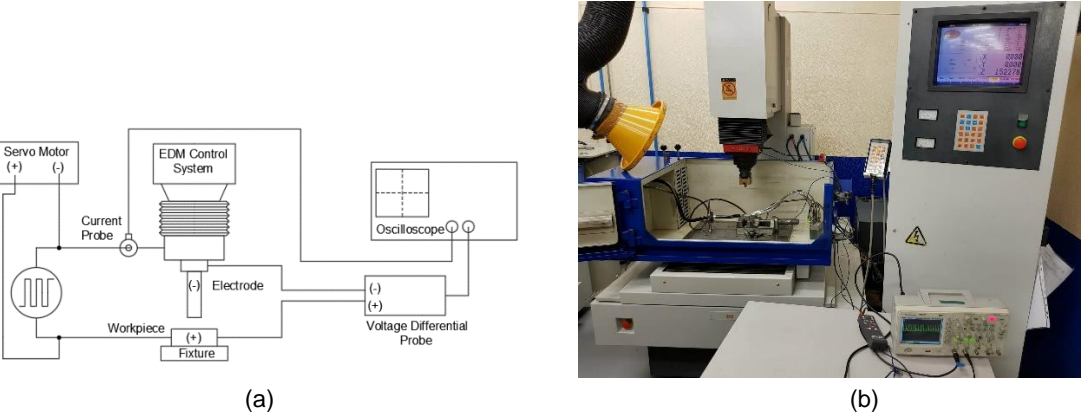


Figure 3-6 - (a) Schematical apparatus; (b) Experimental apparatus.

Apparatus is developed in an industrial machine ACT Spark SP1, a CNC Die-Sinking EDM SP Series, used trough the experiments for machining a pocket on an aluminium alloy 1050A workpiece surface, with a tool-electrode of electrolytic copper. Experiments were carried out with direct current, with the electrode negatively charged, making the aluminium workpiece connected to the positive pole. That lead us to connect the differential probe negative bank to the electrode, and the positive bank to the aluminium workpiece. The current sensor device is placed surrounding the power cable, acquiring values in volts, having a strict relation of 0.5 V/A. Debris flushing inlet, is placed near the electrode

aligned with the width direction, and its outlet is placed in the opposite corner with a suction line for removing debris of the machining zone. Figures 3-6 show us Experimental Apparatus, containing the electrical probes for acquiring EDM electrical signature.

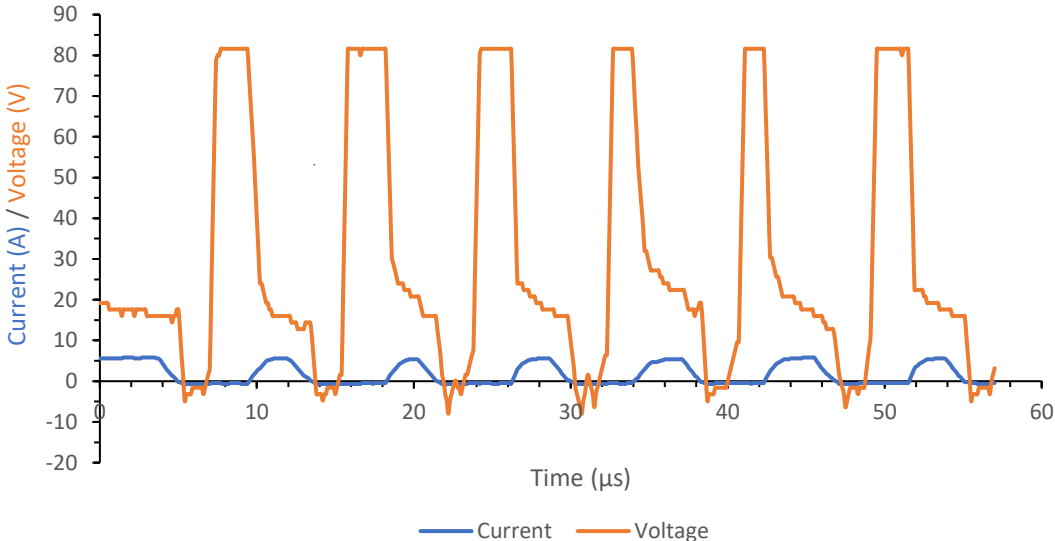


Figure 3-7 - Electrical signature for an open voltage of 80 V, discharge current of 5.6 A, pulse off time of 3 μs and pulse on time of 5 μs.

Figure 3-7 presents an electrical signature for an open voltage of 80 V, and a discharge voltage with a negative rate lying between 30 and 15 V. Pulse off time and pulse on time are 3 μs and 5 μs, respectively, where discharges duration is around 4 μs, and with a current of 5.6 A. Pulse duration and interruption were measured on a preliminary tests phase, because these quantities are set by codes that don't stand for the actual physical values. This is common to industrial machines that work based on technological tables.

During a preliminary tests phase, several experiments were made until we managed to define a suitable machinability region of the material pair of electrode of electrolytic copper and AA1050 A. In figures 3-8 (a) and (b) we may see a machined surface and the respective EDM electrical signature. This experiment was conducted with the flushing jets aligned with the length direction.

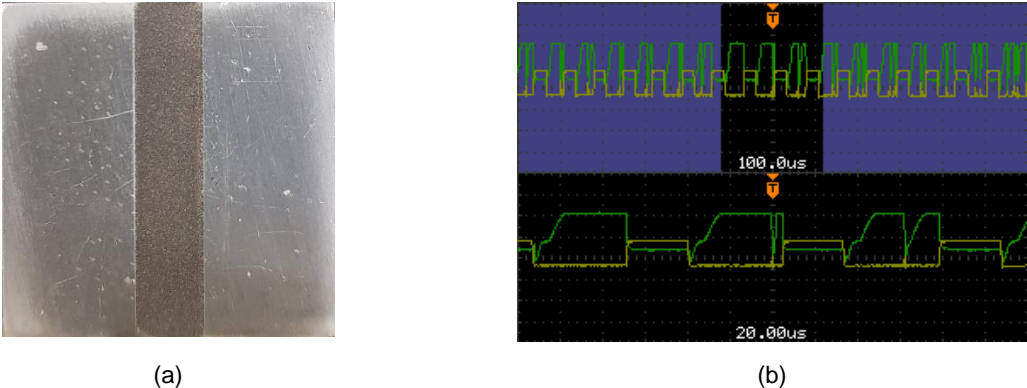


Figure 3-8 - (a) Machined workpiece surface and (b) its respective electrical signature.

This experiment resulted on a non-typical surface finish, with darker colour than the described on the literature, that EDM resulted part has a visible white layer underneath the molten material

spattered in surface, that in this case, wasn't of easy removal. Residues were deeply ingrained creating a dark surface.

### 3.3 Experimental Plan

Once achieved a good parameters control, experimental plan concerning electrical parameters influence can be created. This plan has two project variables (two varying parameters), being these discharge current ( $I_e$ ) and pulse on time ( $T_{on}$ ). Besides these two, all electrical parameters are constant for all experiments. Pulse off time ( $T_{off}$ ) set value was of 3  $\mu s$ , 80 V for open voltage ( $U_o$ ), and discharge voltage ( $U_e$ ) lying between 30 and 15 V. As explained before, this last parameter is uncontrollable [6]. Following table contains experimental plan data parameters.

Table 6 - Electrical parameters influence experimental plan.

Constant Parameters			Varying Parameters	
$U_o$ (V)	$U_e$ (V)	$T_{off}$ ( $\mu s$ )	$T_{on}$ ( $\mu s$ )	$I_e$ (A)
80	[15;30]	3	1	5.6
80	[15;30]	3	1	9.4
80	[15;30]	3	1	14.2
80	[15;30]	3	3	5.6
80	[15;30]	3	3	9.4
80	[15;30]	3	3	14.2
80	[15;30]	3	5	5.6
80	[15;30]	3	5	9.4
80	[15;30]	3	5	14.2

Other experimental plan arises concerning electrode surface roughness influence on the workpiece surface roughness. This experimental plan is performed for constant electrical parameters for all experiments. Electrical parameters combination level is the one that revealed optimum for the electrical parameters influence experimental plan in terms of workpiece SR. Experiments consist in different initial electrode surface roughness achieved by abrasive paper polishing with 5 different granulometries for 3 different machining times, considered as parameters. Process responses to evaluate are then workpiece SR and electrode final electrode SR. Following table contains the inputs electrode roughness influence experimental plan.

Table 7 - Electrode Roughness Influence experimental plan.

Time (min)	30		60		90	
Roughness ( $\mu m$ )	$Ra_{Ei}$	$Rz_{Ei}$	$Ra_{Ei}$	$Rz_{Ei}$	$Ra_{Ei}$	$Rz_{Ei}$
	0.141	0.885	0.151	0.672	0.249	1.516
	0.464	2.662	0.408	2.416	0.478	2.436
	0.795	3.644	0.705	7.105	0.766	3.842
	1.224	7.105	1.049	5.772	1.009	5.518
	1.491	7.491	1.971	8.322	1.771	7.566

## 4 Results

This chapter concerns about results of the tests performed throughout this work, being presented in different subchapters. The first subchapter, where an influence study is made concerning electrical parameters, namely pulse on time and discharge current, looking for the parameter combinations that optimize each of the process response. The second, gives attention to the non-electrical parameters, more specifically to electrode roughness influence for different machining times, aiming to quantify its contribution to the workpiece surface roughness. The third and last subchapter then appears as a machining strategy aiming to reduce the roughness of the machined surface against the optimum result obtained in the first subchapter as well for a better rate of material removal.

### 4.1 Electrical Parameters Influence

Electrical parameters experiments were carried out on a total of 9 tests, to find response values for, surface roughness, material removal rate, electrode wear rate and consequently wear ratio. The chosen varying parameters were pulse on time and discharge current, while open voltage, and pulse off time, where kept constant for all experiments with a respective value of 80 V and 3  $\mu$ s. Discharge voltage normally lies between 15 and 30 V for all experiments. In a practical way, when we perform to a graphical analysis, on a 2D graph, it is more appropriate to take in consideration only two varying parameters, so we can examine in a more certain way, knowing that only two variables are changing while the other ones are kept constant, and so, we can read it properly. The chosen geometry for the experiments was a “pocket”, with a machining area 5x20  $mm^2$ , and a depth of 0,2 mm. Table 8 contains, the parameters values and results, for each experiment.

Table 8 - Electrical parameters experiments results.

Parameters		Responses							
$T_{on}$ ( $\mu$ s)	$I_e$ (A)	$Ra_W$ ( $\mu$ m)	$Rz_W$ ( $\mu$ m)	$Ra_{Ef}$ ( $\mu$ m)	$Rz_{Ef}$ ( $\mu$ m)	$T_{mach}$ (min)	MRR (g/min)	EWR (g/min)	WR
1	5.6	1.306	7.387	0.373	2.275	127.23	0.000503	7.86E-05	0.047
1	9.4	1.551	8.739	0.543	3.274	33.483	0.0022	0.000358	0.049
1	14.2	2.144	11.09	0.602	3.581	18.25	0.002192	0.000493	0.068
3	5.6	1.491	7.971	0.462	2.754	66.35	0.000603	0.000106	0.053
3	9.4	2.266	10.94	0.619	3.782	7.43	0.005291	0.000728	0.042
3	14.2	2.65	12.26	0.676	3.888	6.1	0.008689	0.001475	0.052
5	5.6	1.828	9.067	0.556	3.227	41.35	0.000846	0.000129	0.046
5	9.4	2.492	11.44	0.682	3.917	5.65	0.006844	0.001003	0.044
5	14.2	3.354	14.12	0.78	4.462	3.55	0.015211	0.002254	0.045



As above presented,  $T_{off}$  is equal for all experiments, but  $T_{on}$  has three different values, leading to three different cyclic relationship. Cyclic Relationship stands for the ratio of  $T_{on}$  and the sum of  $T_{off}$  and  $T_{on}$ . The Cyclic Relationship can be described by equation 12. Tables 9 and 10 contain the proof body aesthetics after machining, as well for their view on digital microscopic.

Table 9 - Workpiece microscopic view for the different electrical parameters. Note, real width dimension equal to 0.25 mm.

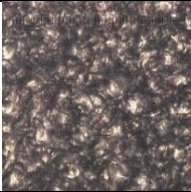
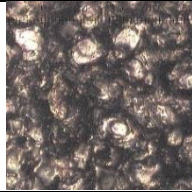

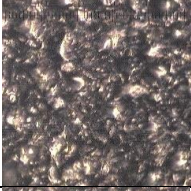


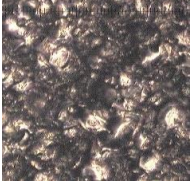




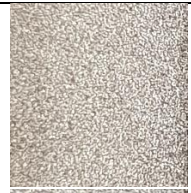






		Pulse On Time ( $\mu$ s)		
		1	3	5
Discharge Current (A)	5.6			
	9.4			
	14.2			

Table 10 - Workpiece aesthetics for the different electrical parameters.

		Pulse On Time ( $\mu$ s)		
		1	3	5
Discharge Current (A)	5.6			
	9.4			
	14.2			

$$\alpha = \frac{T_{on}}{T_{off} + T_{on}}; \tag{12}$$

Table 11 - Electrode microscopic view for the different electrical parameters. Note, real width dimension equal to 0.25 mm.


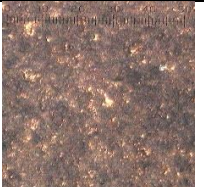







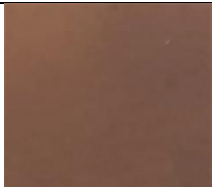
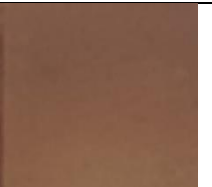



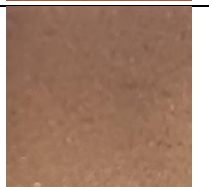
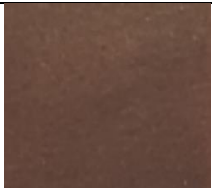
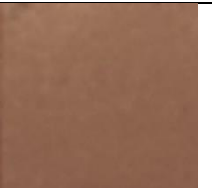
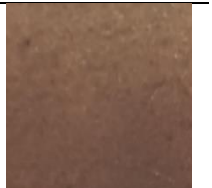
		Pulse On Time ( $\mu\text{s}$ )		
		1	3	5
Discharge Current (A)	5.6			
	9.4			
	14.2			

Table 12 - Electrodes surface after machining for the different electrode parameters.

		Pulse On Time ( $\mu\text{s}$ )		
		1	3	5
Discharge Current (A)	5.6			
	9.4			
	14.2			

By the figures presented in tables above 11 and 12, it is clear while increasing Discharge Energy, meaning with higher levels of  $I_e$  and  $T_{on}$ , craters generated on the workpiece by machining operation present a larger width when compared to lower discharge Energy. The same is denoted on the electrode but with lower perception than in the workpiece. In addition, we may say that in aesthetical terms lower  $I_e$  and  $T_{on}$  induce on a more appealing view.

Once this study is mainly focused on finishing operations environment we'll start for presenting surface roughness relationship with electrical parameters. Surface roughness has several parameters, like Ra and Rz, explained before on sub chapter process responses, and these were accounted for relating SR with the electrical Parameters that characterize EDM material removal mechanism. Different notations appear like,  $Ra_w$ ,  $Ra_{Ei}$ ,  $Ra_{Ef}$  and are used to differentiate arithmetical mean workpiece roughness and electrode initial or final roughness. The same happens for differentiate maximum surface roughness.

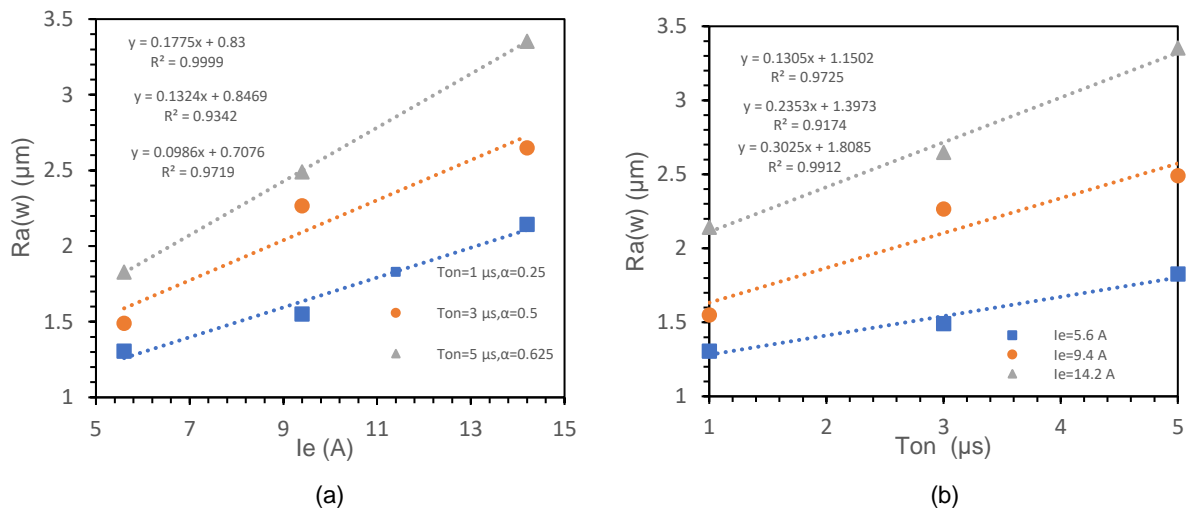


Figure 4-1 - Relationship between  $Ra_w$  and electrical parameters, for an open voltage of 80 V and pulse off time of 3  $\mu s$ .

By figure 4-1, we denote an approximately linear relationship between  $Ra_w$  and discharge current and pulse on time, where whenever  $I_e$  and  $T_{on}$  increase, higher will be  $Ra_w$  value. These results show a conformity relation with discharge energy ( $W_e$ ), that is mainly affected by voltage, current and duration of discharge, that when is low, a smaller amount of material is removed, meaning that smaller craters will be generated on the machining operation. Optimum levels in terms of  $Ra_w$  are identified, being these 1  $\mu s$  of  $T_{on}$  and 5.6 A of  $I_e$ , with the lower  $W_e$  of the experimental plan.

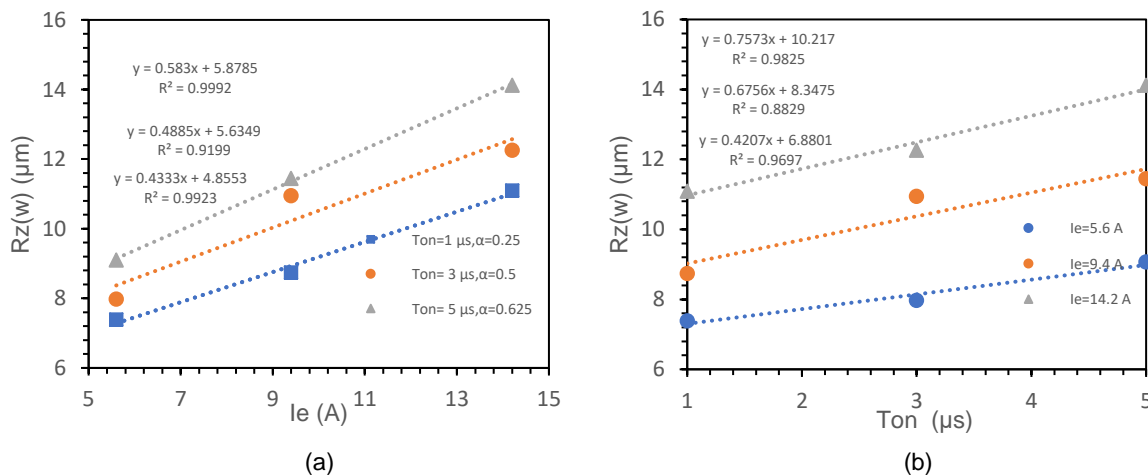


Figure 4-2 - Relationship between  $Rz_w$  and electrical parameters, for an open voltage of 80 V and pulse off time of 3  $\mu s$ .

Summarizing, lower SR is achieved minimizing discharge energy that is strictly related to discharge current and discharge duration.  $T_{on}$  is composed by two stages, the ignition delay where dielectric fluid is ionized in the gap between tool and workpiece creating an electrical field attracting microscopic contaminants creating a high conductivity bridge. With this, discharge occurs and is only interrupted when  $T_{on}$  level pre-set completes its duration. Examining  $Ra_W$  and  $Rz_W$  relations between electrical parameters, where we conclude lower Discharge Energy leads to minimum  $Ra_W$  and  $Rz_W$ , a last experiment is performed for a Discharge Current level of 0.8 A, and it is presented on Technological Approach sub chapter. In order to evaluate  $Ra_W$  relationship with  $Rz_W$ , these two are plotted together in the same graph. This intends to examine Aluminium SR behavior.

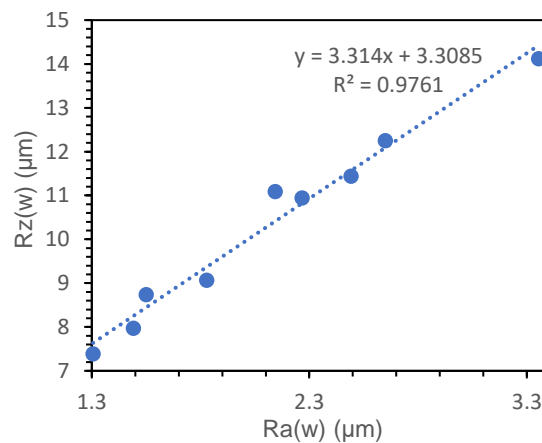


Figure 4-3 - Relationship between  $Ra_W$  and  $Rz_W$

Relationship between  $Ra_W$  and  $Rz_W$  show a positive correlation coefficient, with a  $Rz_W$  growth higher than  $Ra_W$ .  $Rz_W$  evolution tends to be of higher growth rate while increasing  $I_e$  and  $T_{on}$ , that increase  $W_e$  resulting in deeper craters. Besides workpiece surface roughness, initial and final electrode roughness are considered, where electrodes are polished in order to guarantee a smooth surface as initial condition. Still, there are significant differences in terms of initial electrode surface roughness. 2D plots of  $Ra_{Ef}$  are presented in figure 4-4.

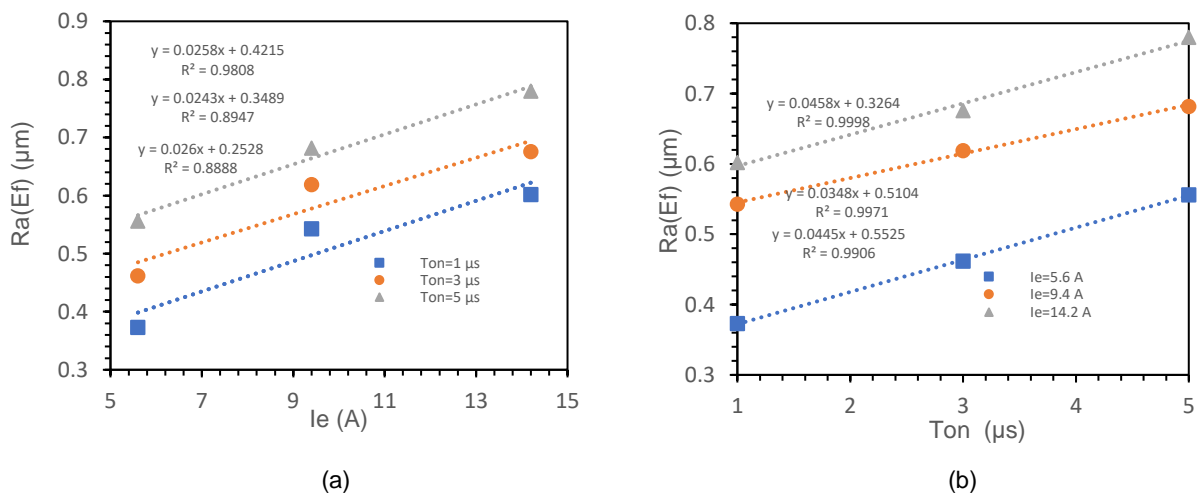


Figure 4-4 - Relationship between  $Ra_{Ef}$  and electrical parameters, for an open voltage of 80 V and pulse off time of 3 µs.

For all parameter level combinations,  $Ra_{Ef}$  is smaller than  $Ra_W$ . This difference in results between electrode and workpiece, when compared with microscopic view of surfaces presented in tables 9 & 11 are reasonable, once craters are more perceptible in the workpiece microscopic views than in the ones presented for the electrode. As craters are smaller in the electrode than in the workpiece, electrode wear rate is expected to be of less quantity than material removal rate.  $Rz_{Ef}$  relationship with electrical parameters is also accounted and is presented in figure 4-5.

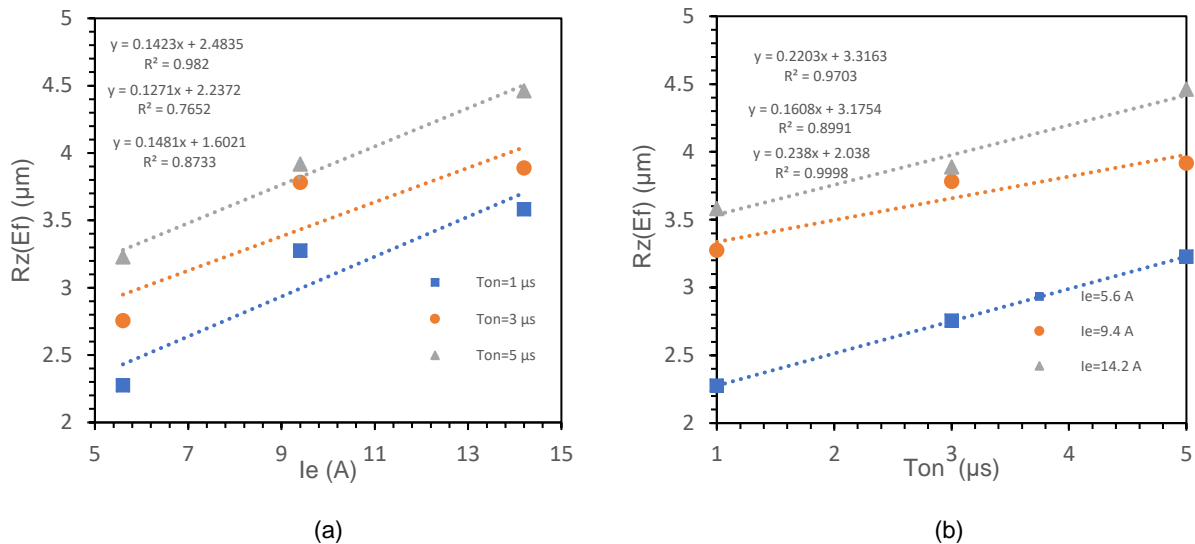


Figure 4-5 - Relationship between  $Rz_{Ef}$  and electrical parameters, for an open voltage of 80 V and pulse off time of 3  $\mu s$ .

Once presented  $Rz_{Ef}$  relationship with electrical parameters we can, in a general mode, conclude that the optimum SR values are achieved minimizing  $W_e$ , more specifically in the parameter combination level of 5.6 A of  $I_e$  and 1  $\mu s$  of  $T_{on}$ . This is a valid conclusion for the workpiece, as well for the electrode. Similarly, to the workpiece SR, where we plot  $Rz_W$  with  $Ra_W$  in order to understand their relation,  $Rz_{Ef}$  and  $Ra_{Ef}$  are also plotted together.

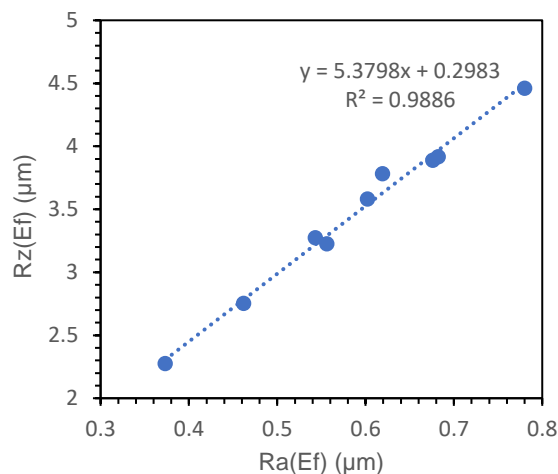


Figure 4-6 – Relationship between  $Rz_{Ef}$  and  $Ra_{Ef}$ .

Like in the relationship between  $Ra_W$  and  $Rz_W$ ,  $Ra_{Ef}$  and  $Rz_{Ef}$  relationship shows a linear positive correlation coefficient, with a more accentuated growth, even  $Rz_W$  is far higher  $Rz_{Ef}$ .



Looking now to Material Removal Rate, the amount of material removed per time unit, an optimum result would be the parameters combination that lead us to its maximum value. MRR 2D plots are presented in figure 4-7.

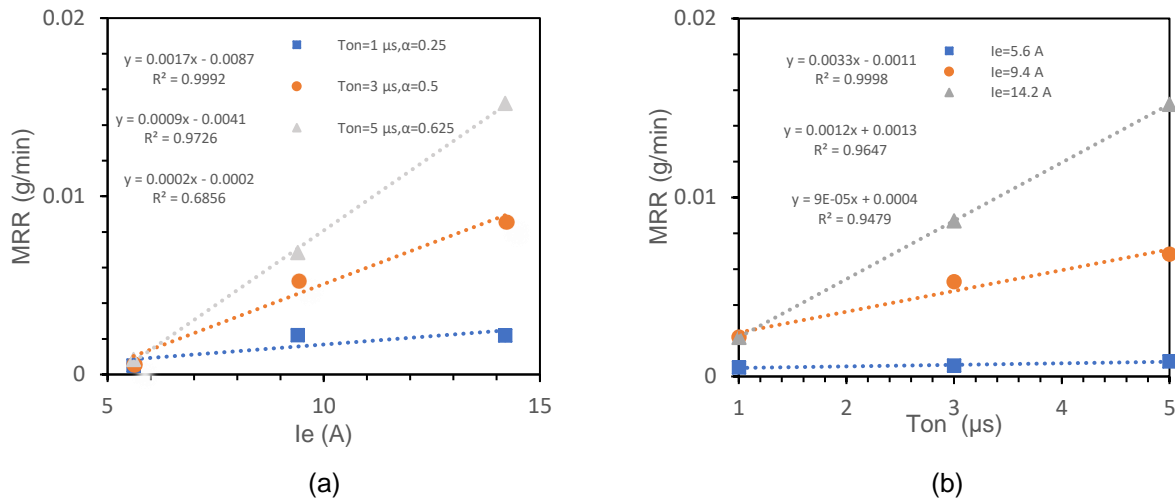


Figure 4-7 - Relationship between MRR and electrical parameters, for an open voltage of 80 V and pulse off time of 3 μs.

Looking to MRR relationship with electrical parameters, its maximum is obtained at the higher levels of  $I_e$  and  $T_{on}$ . There is some conformity with this assumption and the one presented by [5], [10] and [11], referenced on this document Process Responses sub chapter. In addition, we may say that at 5.6 A, MRR present similar values for the different  $T_{on}$  presenting an almost constant evolution, but when  $I_e$  increases, MRR values increase and tend to disperse. Optimum point is graphically identified to be 14.2 A of  $I_e$  and 5 μs of  $T_{on}$ . Looking to tables 9 & 10, we denote a far poorer surface finish than the one presented as optimum in terms of Ra. Once this is the optimum MRR value and was obtained with the higher level of discharge energy, craters are easily identified to be wider than the optimum machined surface in terms of Ra. Besides MRR, EWR is accounted on this study, looking to understand its behaviour when subjected to different levels of  $I_e$  and  $T_{on}$ . Similar to MRR, EWR is higher for the higher levels of Discharge Energy, but this EDM process response is known to be optimum when it presents its smaller value. EWR 2D plots are presented in figure 4-8.

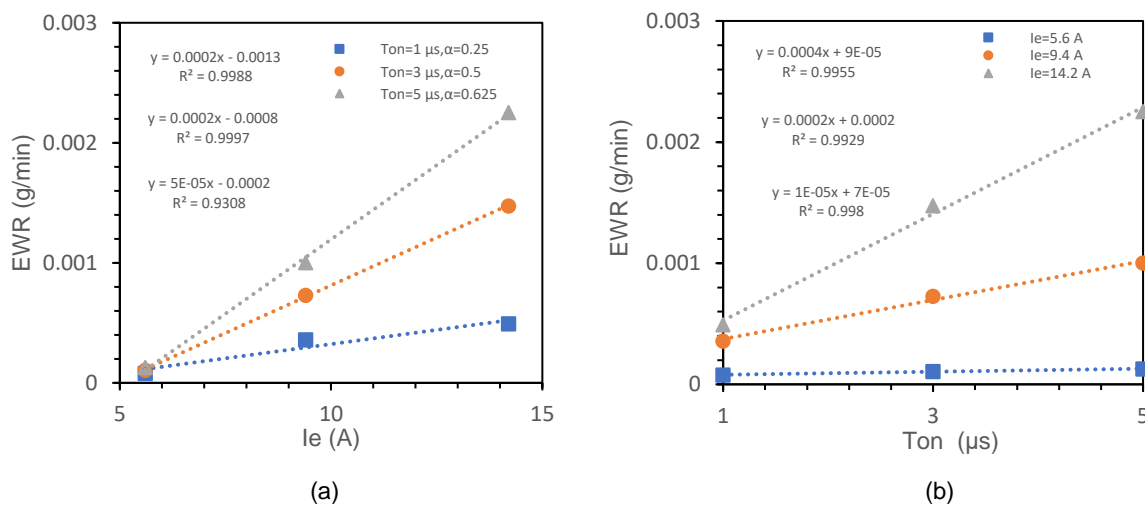


Figure 4-8 - Relationship between EWR and electrical parameters, for an open voltage of 80 V and pulse off Time of 3 μs.

Analysing EWR relationship with electrical parameters, we denote an approximately linear evolution, where EWR increases with discharge current increase. Like MRR, EWR presents similar values at  $I_e$  at 5.6 A, for the three different  $T_{on}$  levels, that can be seen in figure 4-8 (b). Increasing  $I_e$ , EWR values disperse where  $T_{on}$  at 1  $\mu s$  present us its lower value. Furthermore, by graphical observation EWR optimum point is 5.6 A and 1  $\mu s$ .

EWR, Ra and Rz revealed the optimum value at the same parameters level combination, making it the adequate parameters set for a finish pass, although this combination results in the lower MRR value. To complete EDM process responses, Wear Ratio must be examined, being this the combined value of EWR and MRR, that stands for the ratio between them, and is extreme importance because plays an indispensable role in economic terms, and its optimum result stands for the lower value. The results presented in this analysis are ruled by equation 13.

$$WR = \frac{EWR}{MRR} \times \frac{\rho_{workpiece}}{\rho_{electrode}} \quad (13)$$

2D plots of WR relationship with  $I_e$  and  $T_{on}$  are presented in the figures below.

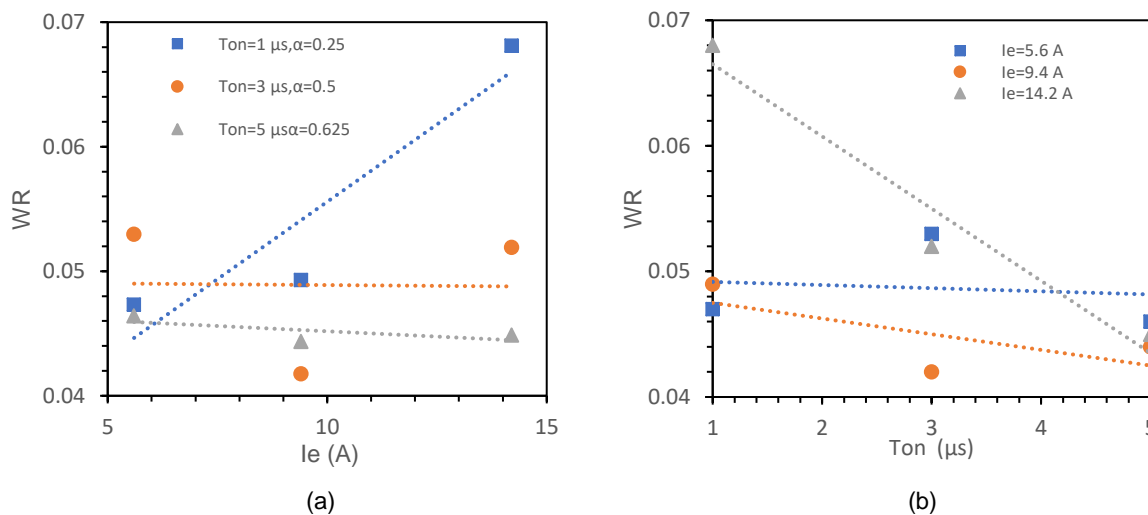


Figure 4-9 - Relationship between WR and electrical parameters, for an open voltage of 80 V and pulse off time of 3  $\mu s$ .

Wear Ratio presents a more disperse data than the other process responses, and it was to be expected since it results from a ratio of two other process responses. These results, generally contradict the assumption presented by Khan, that WR decreases with  $I_e$ , once at  $T_{on}$  at 1  $\mu s$  we see a gradual increase of WR while increasing  $I_e$ , and it may be explained by the fact that a lot of power input is being generated and aluminium specific heat ( $J/(kg.K)$ ) is far higher than copper, and for that low  $T_{on}$  temperature increase will be lower than other  $T_{on}$  levels and it removes a lower amount of material.  $T_{on}$  at 5  $\mu s$ , shows a tendency of a soft linear decrease with an almost negligible difference between values, revealing the lower WR values.  $T_{on}$  at 3  $\mu s$  present a minimum local at mean level of  $I_e$ , while at lower and higher level of  $I_e$  they present similar WR values. By graphical inspection, WR minimum should indicate the optimum point, but for our tendency lines  $T_{on}$  at 5  $\mu s$  has already revealed itself as optimum. In addition, we may refer that WR presents fluctuating minimums when combined for different levels of

$I_e$  and  $T_{on}$ . When looking to figure 4-9 (b)  $I_e$  at 9.4 A presents, in average the lower WR values, and for figure 4-9 (a), lower values of WR are in average at 5  $\mu s$   $T_{on}$ . Signal to noise (S/N) ratio and data means will help us to confirm our optimum parameters combination level. "Smaller the better" is the correlation function used, for WR is a process response we intend to minimize. Maximums on S/N ratio plots are the ones who minimize WR, while in data means, lower values indicate our optimum parameter level.

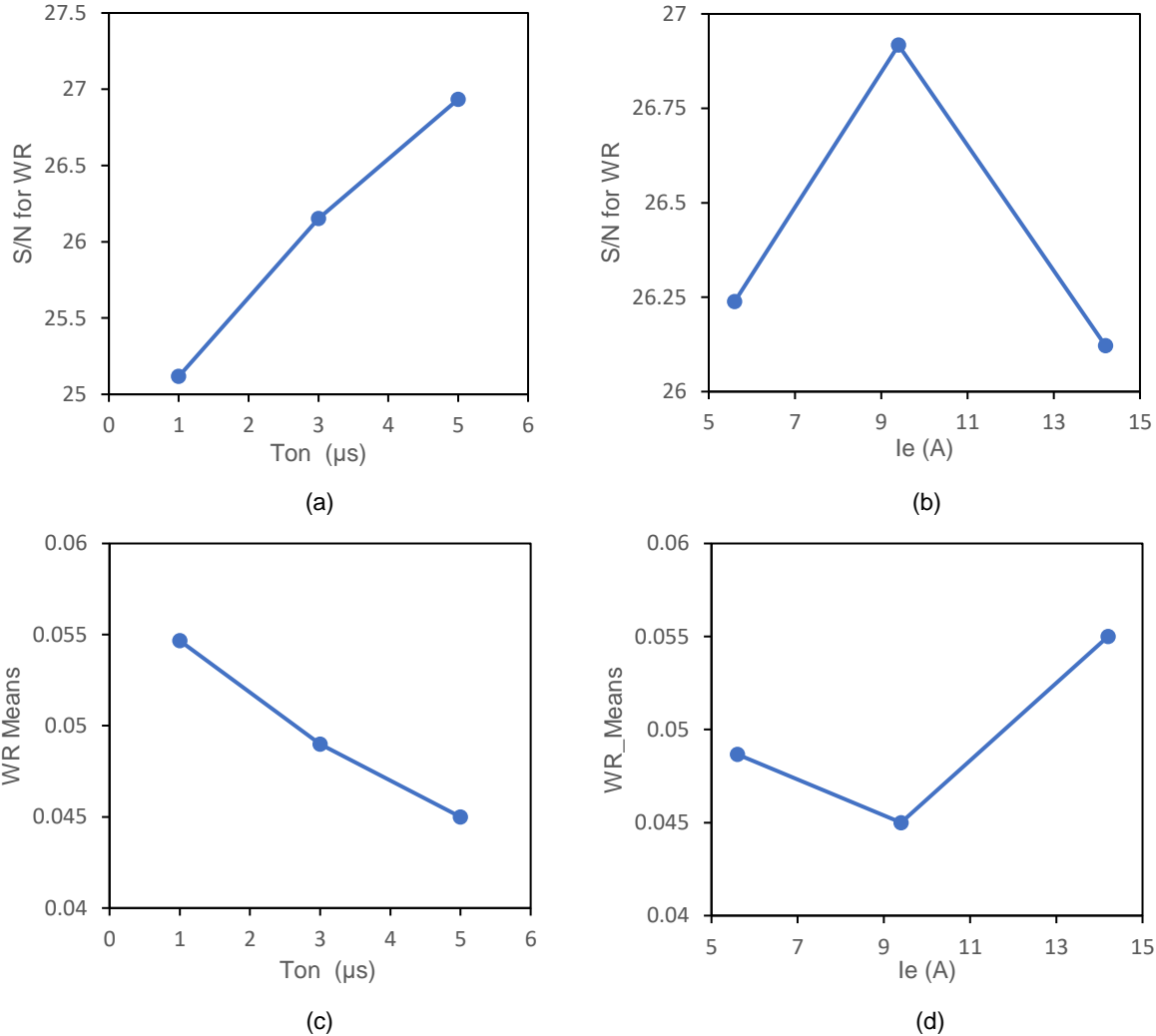


Figure 4-10 – (a) & (b) S/N plot and (c) & (d) Data means for WR.

According to S/N and Data Means for WR, optimum parameters combination level is identified to be at 5  $\mu s$  of pulse on time and 9.4 A of discharge current. To interpret mean level of discharge current as optimum is reasonable, once it moderates the amount of energy carried on discharges that occur in EDM process.

### 4.2 Electrode Roughness Influence

EDM is a material removal mechanism, where there is no mechanical contact between tool and workpiece. In Die-Sinking variant, the inverted electrode geometry is gradually printed on the workpiece, meaning that electrode geometry is being copied to the workpiece. This section concerns about the electrode roughness impact on the workpiece surface, looking to evaluate its influence on surface finish, importance degree, levels of stability and growth. For this, a new experimental plan is conceived where



all experiments are carried with the same electrical signature, with the optimum levels of discharge current and pulse on time in terms of Ra in the previous analysis (5,6 A and 1  $\mu$ s). Experimental plan consists in three different machining times, having each of these, 5 tests with different electrode initial surface roughness. Electrode initial roughness values vary, because they are obtained by abrasive paper polishing (5 different granulometries). The experimental plan and respective results are presented in table 13.

Table 13 - Electrode roughness influence experimental plan and respective data.

Parameters			Responses			
Machining Time	Ra <sub>Ei</sub> ( $\mu$ m)	Rz <sub>Ei</sub> ( $\mu$ m)	Ra <sub>Ef</sub> ( $\mu$ m)	Rz <sub>Ef</sub> ( $\mu$ m)	Ra <sub>W</sub> ( $\mu$ m)	Rz <sub>W</sub> ( $\mu$ m)
30 min	0.141	0.885	0.552	3.207	1.256	7.753
	0.464	2.662	0.55	3.162	1.228	7.287
	0.795	3.644	0.648	3.868	1.305	7.857
	1.224	7.105	0.919	3.851	1.511	8.763
	1.491	7.491	1.074	5.792	1.467	7.971
60 min	0.151	0.672	0.448	2.735	1.26	6.981
	0.408	2.416	0.415	3.069	1.235	9.197
	0.705	7.105	0.63	3.944	1.379	9.026
	1.049	5.772	0.841	4.545	1.588	8.01
	1.971	8.322	0.999	8.207	1.62	10.036
90 min	0.249	1.516	0.721	3.949	1.427	8.201
	0.478	2.436	0.709	3.782	1.407	8.064
	0.766	3.842	0.742	3.851	1.346	7.837
	1.009	5.518	0.842	4.545	1.668	9.317
	1.771	7.566	0.904	5.154	1.745	9.802

#### 4.2.1 Workpiece Roughness Evolution

This subchapter concerns about electrode roughness influence on aluminum workpiece machined surface. With no previews studies found on bibliography, here we intend to understand if it has some significant influence, once a small amount of Discharge Energy (~100  $\mu$ J) is carried on these 15 experiments, reminding optimum parameters combination level found on previews subchapter, Electrical Parameters Influence is used, that induce on a low EWR. With a low EWR, electrode will preserve, or lose a small amount of its roughness created by lower granulometry abrasive paper, and with this deeper valleys or peaks of electrode surface will be copied, but inverted, to the aluminium workpiece machined surface. If we pay careful attention to the figure following presented, some scratches can be observed, aligned with horizontal direction, being copied from electrode, and that's not a typical property of an EDM machined surface, that normally is composed by an intersection of multiple craters.



(a)



(b)



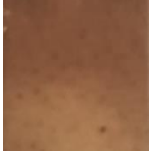



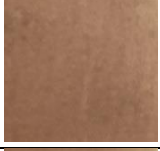
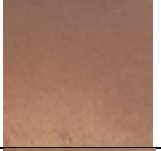
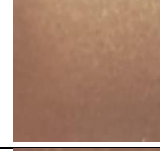




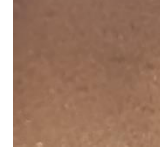

Figure 4-11 – Proof body after machining for an experiment of 90 minutes with a rough electrode. (a) Electrode after machining; (b) Workpiece machined surface.

In figure 4-11, we may see some protrusions and recesses copied from the electrode. Figure 4-12 illustrates workpiece surface roughness behavior, when submitted to different machining times and electrode surface roughness. SR parameter chosen to characterize electrode roughness influence is  $R_a$ , arithmetical mean surface roughness.

Table 14 - Workpieces machined during electrode influence experiments.

		$R_{a_{Ei}}$ ( $\mu\text{m}$ )				
		[0.15;0.25]	[0.4;0.5]	[0.7;0.8]	[1;1.2]	[1.5;2]
Machining Time (minutes)	30					
	60					
	90					

Table 15 - Electrodes used during electrode influence experiments.

		$Ra_{Ei}$ ( $\mu\text{m}$ )				
		[0.15;0.25]	[0.4;0.5]	[0.7;0.8]	[1;1.2]	[1.5;2]
Machining Time (minutes)	30					
	60					
	90					

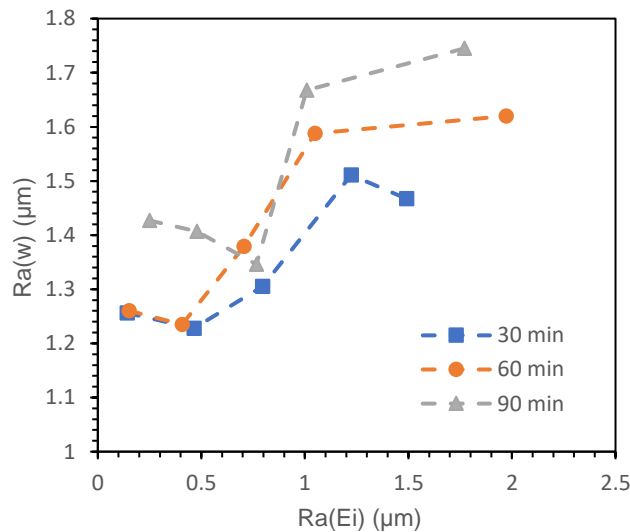


Figure 4-12 - Electrode surface roughness influence on workpiece machined surface.

Here, we may see electrode surface finish plays an important role, having its mark well defined on Workpiece Roughness ( $Ra_w$ ), making a good point, once the electrode negative geometry is machined on the workpiece.

In general,  $Ra_w$  grows for larger  $Ra_{Ei}$  and machining time values, presenting a behavior with 3 different phases. The first phase,  $Ra_w$  doesn't vary significantly its value leading us to think it is Steady, the second phase where it presents an approximately linear evolution region, and the third phase, it reaches its limit and tend to stabilize.

These three regions, are clearly illustrated in figure 4-12, easily identified for 30 and 60 minutes of machining time. Machining time at 90 minutes, presents us a valley before growth region, contradicting the general conclusion, that  $Ra_w$  tends to increase for larger machining times and  $Ra_{Ei}$ . Through this analysis, it is denoted the importance of electrode finish quality and how influent it is on the workpiece finish. The following graph illustrates  $Ra_w$  evolution trough time, in a total of 5 series gathering an average of 3  $Ra_{Ei}$  (due to 3 different machining times), being each of these 5-series

polished with 5 different granulometries. This plot intends to bring a better understanding to Electrode Roughness Influence.

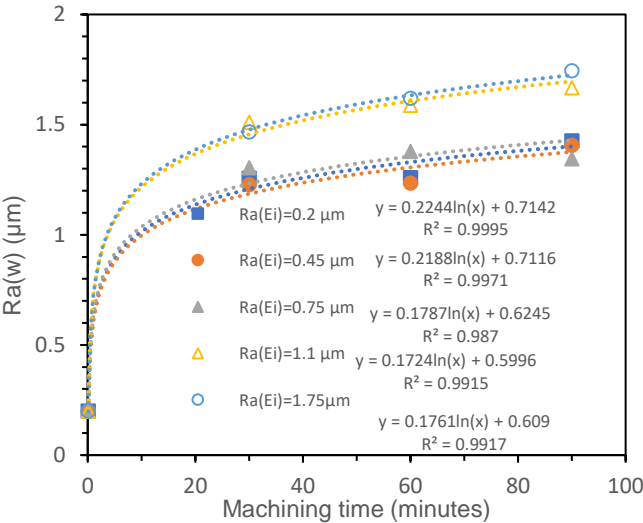


Figure 4-13 - Electrode roughness influence.

This approach presents a logarithmic evolution, where the rougher electrode increases  $Ra_w$  when compared with electrodes with relative lower initial roughness. Empirical equations generated appear in the shape of the following equation:

$$Ra_w = C_1 \ln(x) + C_2 \tag{14}$$

It is denoted that the three less rougher electrodes present a similar evolution and it can be graphically seen, and as well for tendency lines, where constants  $C_1$  and  $C_2$ , present a small difference between them. The rougher series have a larger step towards the first three polished series, but present similar  $C_1$  and  $C_2$  between them. 5 equations are obtained for the different 5 initial electrode roughness. A new graph is created, by plotting  $C_1$  and  $C_2$  function of initial electrode roughness and is following presented.

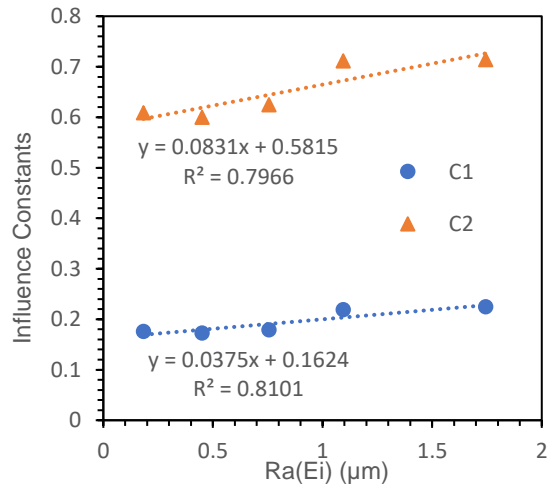


Figure 4-14 - Plot of influence constants vs initial electrode average surface roughness.




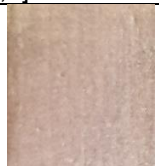
This graph above presented is named influence constants, for it plays a role of electrode roughness influence on the workpiece surface roughness.  $C_1$  and  $C_2$  equations are following presented.

$$C_1 = (0.0375 * Ra_{Ei} + 0.1624) \quad (15)$$

$$C_2 = (0.0831 * Ra_{Ei} + 0.5815) \quad (16)$$

Two last tests are performed, aiming to understand if roughness stabilizes, with the rougher and the most polished series of electrodes for 240 minutes of machining time. Results to these tests are presented in the following table and graph, with the omitted intermediate electrode series.

Table 16 – Workpieces and electrodes for experiments of 240 minutes.

		Ra <sub>Ei</sub> (μm)			
		[0.15;0.25]		[1.5;2]	
Machining Time (minutes)	240				

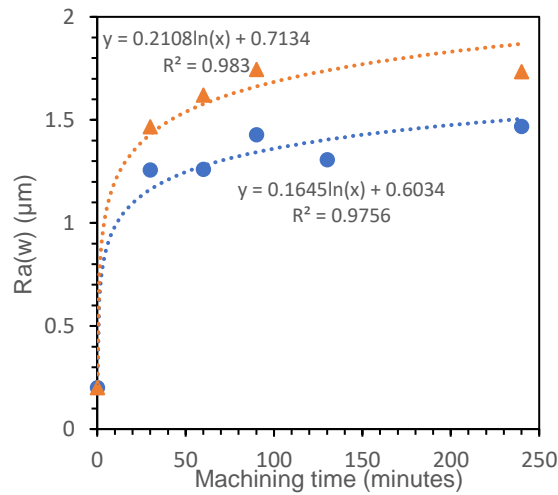








Figure 4-15 - Workpiece surface roughness evolution.

These two last experiments were performed, figure 4-15, intending to understand if  $Ra_w$  stabilizes after a certain machining time meeting at the same SR value. For these results, we still denote a significant difference between the rougher and the most polished electrode, even with a small decrease from 90 to 240 minutes of machining time. In addition, we may compare the  $Ra_w$  result from electrical parameters influence, at 130 minutes of machining time.

Three extra experiments were performed, with a polished electrode, but now with a rough workpiece with an  $Ra_{wi}$  of 2.231  $\mu\text{m}$ . Results presented in figure 4-16 plotted together with the previous series machined with a polished electrode shown an almost mirror shaped evolution, converging for the same value after a machining time of 90 minutes.

Table 17 - Experiments for a polished and a rougher workpiece as initial condition with polished electrodes.

		$Ra_{wi}$ ( $\mu\text{m}$ )	
		0.2	2.231
Machining Time (minutes)	30		
	60		
	90		

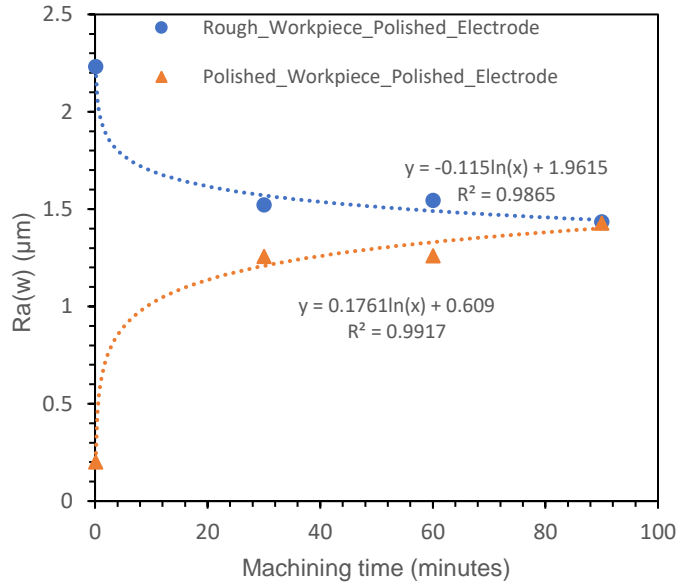


Figure 4-16 - Workpiece roughness evolution.

#### 4.2.2 Electrode Roughness Evolution

Similarly, to Workpiece Evolution, Electrode Roughness shows a tendency of varying its behavior, which can also be separated in three different regions, presented in figure 4-17.

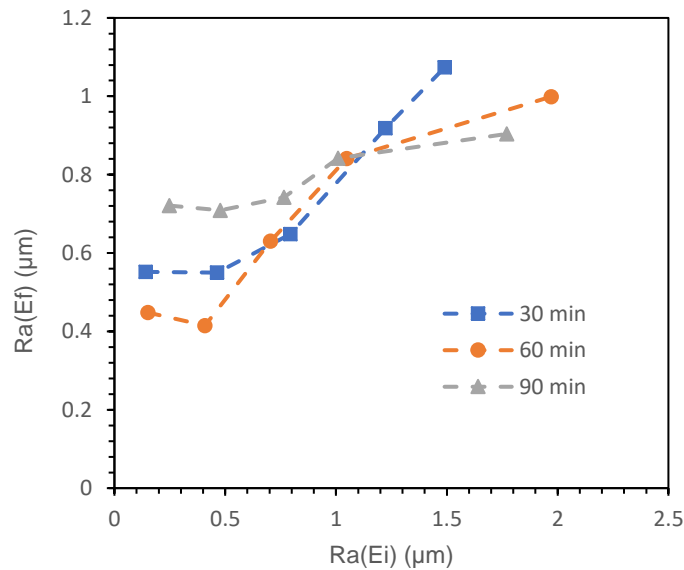


Figure 4-17 - Electrode surface roughness evolution.

The first region, where Final Electrode Roughness is approximately constant, followed by a growth or second region, and a last, where Roughness tends to stabilize. This behavior is perfectly illustrated for machining times of 60 and 90 minutes, while for 30 minutes of machining time, Electrode Final Roughness still didn't reach its limit, with no perception of a "third region" existence. For 90 minutes of machining, a smaller variation is observed when compared with 30, and 60 minutes series, and this may indicate a saturation limit of Surface Roughness. It can also be observed for the three machining times, that for a certain value of initial roughness, final roughness is smaller than its initial. But, it is still

questionable the electrode roughness growth direction in terms of machining time. Approach of data plotting with machining time as the abscises axis was taking in account in this analysis, again for a better understanding of surface roughness.

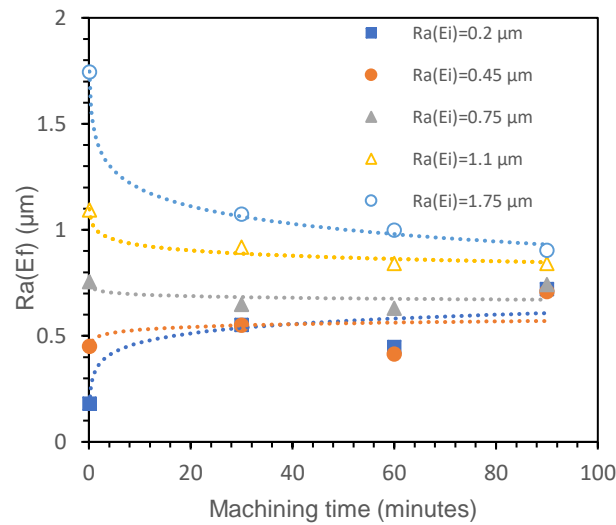
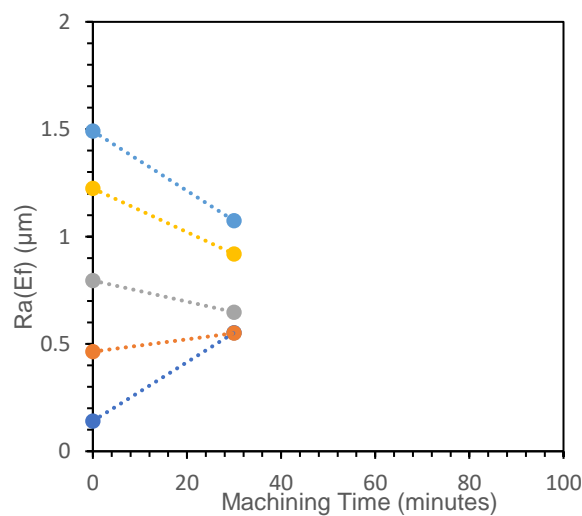


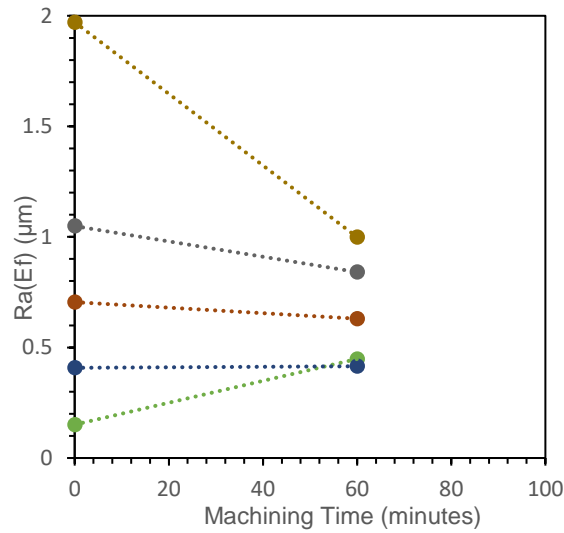
Figure 4-18 - Electrode surface roughness evolution.

In this arrangement, we denote that Electrode Roughness converge asymptotically to a certain value, showing a tendency to stabilize while increasing machining time. We also can see that the two electrodes with the lowest initial roughness, present similar floating results, with a tendency to increase while increasing machining time. Electrode with initial roughness around 0.75 μm, presents an approximately constant evolution with a small variation, giving an idea that it is steady. The two electrodes with higher initial roughness, present a negative rate, while increasing machining time, stabilizing and tending to approximate their roughness values after a certain time. In addition, we may refer less rougher electrodes present a considerable data dispersion and for that reason, real values are presented in figures 4-19 (a)-(c).

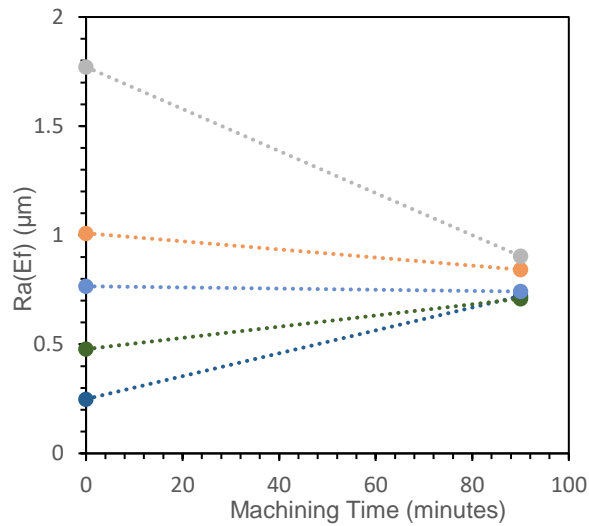


(a)





(b)



(c)

Figure 4-19 - Electrode roughness evolution. (a) 30 minutes, (b) 60 minutes, (c) 90 minutes.

Looking to these simplified electrode roughness evolutions for different machining times, we can clearly affirm the levels where roughness increases, decreases or tends to stabilize. Rougher electrodes clearly decrease their roughness value for all machining times where at 90 minutes present close values, while the most polished always increase their roughness where their final roughness is almost equal for all machining times. Electrode roughness series comprehended between 0.7 and 0.8  $\mu\text{m}$ , can be considered steady or stable for its variation is minimum where it only decreases for 30 minutes of machining time, and for 90 minutes it presents an almost equal roughness value when compared to the most polished electrodes.

In section 4.2.1 were presented two last experiments for a machining time of 240 minutes, for the rougher and the most polished electrodes.  $Ra_{EF}$  with this machining time is presented on the figure below.

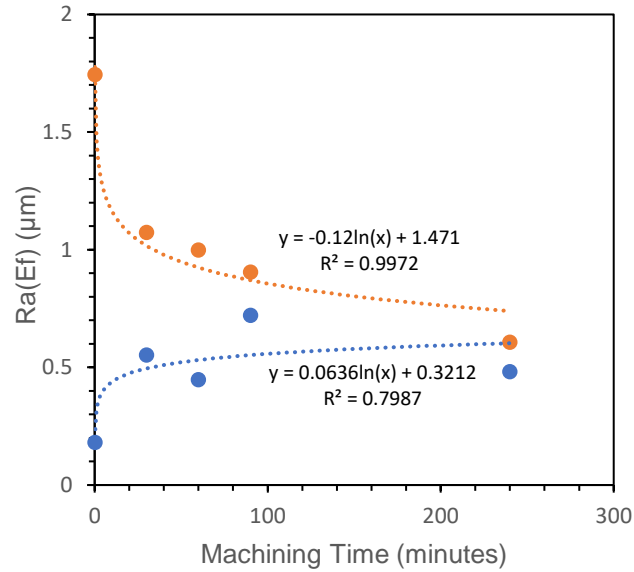


Figure 4-20 - Electrode surface roughness evolution.

$Ra_{EF}$  tend to approximate their final values, presenting a small offset by an approximate value of  $0.1 \mu\text{m}$ . This is a smaller “amount” of roughness, leading us to conclude there is in fact a convergence behavior in terms of electrode roughness.

The data resulted for experiments concerning electrode roughness influence were adjusted to the equations labelled with number (17) and (18), whose correspond respectively to  $Ra_W$  and  $Ra_{Ef}$  behaviors with machining time and  $Ra_{Ei}$ . Figure 4-21 and 4-22, present  $Ra_W$  and  $Ra_{Ef}$  behavior according to the adjusted model equations (17) and (18), together with experimental data.

$$Ra_W = 0.228093 + 0.443687 \ln(T_{mach}) - 0.033598 \ln(T_{mach})^2 + 0.1904867 \ln(Ra_{Ei}) + 0.067069 \ln(Ra_{Ei}^2) \quad (17)$$

$$Ra_{Ef} = 0.07133465 + 0.1132505 \ln(T_{mach}) + 0.9548 Ra_{Ei} - 0.00865 \ln(T_{mach})^2 - 0.0247758 Ra_{Ei}^2 - 0.137 \ln(T_{mach}) Ra_{Ei} \quad (18)$$

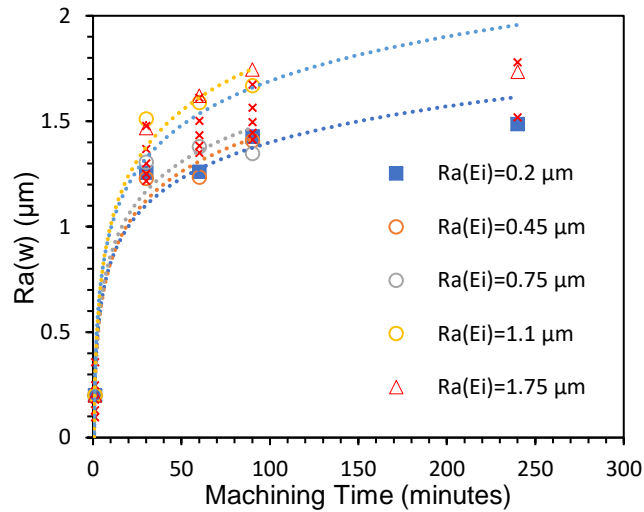


Figure 4-21 - Workpiece surface roughness evolution plotted with model equation.

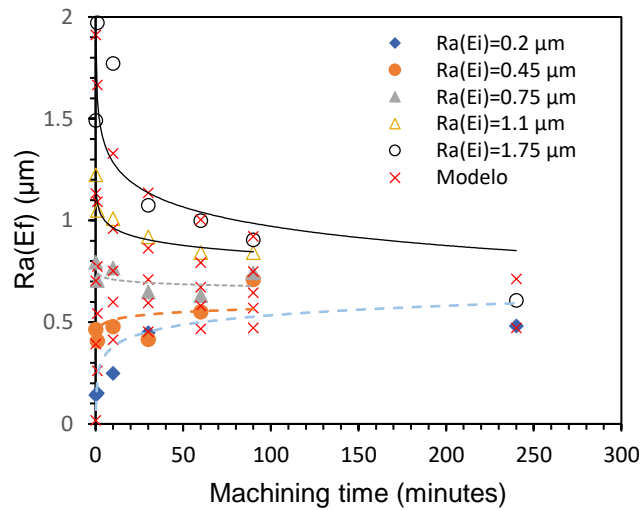


Figure 4-22 - Electrode surface roughness evolution plotted with model equation.

### 4.3 Optimization & Technological Approach

As presented before this study is mainly focused on finishing machining operations, giving special attention to surface roughness. This is the process response we intend to minimize, where the parameters selection is based on the conclusions to the electrical parameters influence. In section 4.1 we concluded that the lower  $W_e$ , the lower SR, meaning that is achieved for lower levels of  $I_e$  and  $T_{on}$ . With this, experiment is conducted with 0.8 A and  $1\mu s$ , and again for a polished electrode for in section 4.2, we concluded the smaller  $Ra_{Ei}$  the smaller  $Ra_w$ . This experiment resulted on a smaller  $Ra_w$  with a value of  $0.612\ \mu m$ . Although a smaller  $Ra_w$  is achieved, machining time was around 9.5 hours, and aesthetical of machined workpiece surface presents some black dots standard being difficult to identify its cause. This black dot standard, common to both surfaces, is presented in the following figures with proof body.

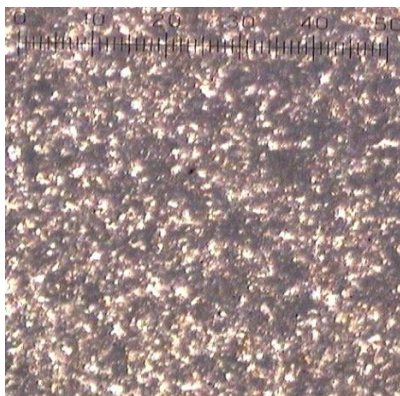


(a)

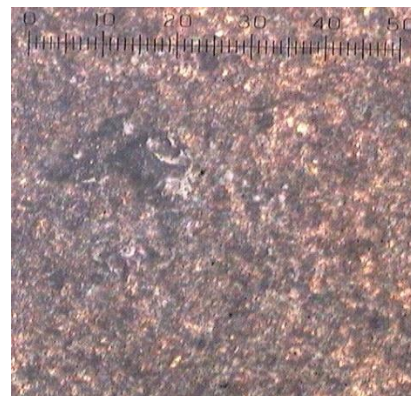


(b)

Figure 4-23 - Optimization experiment. (a) Workpiece machined surface and (b) Electrode machined surface.



(a)



(b)

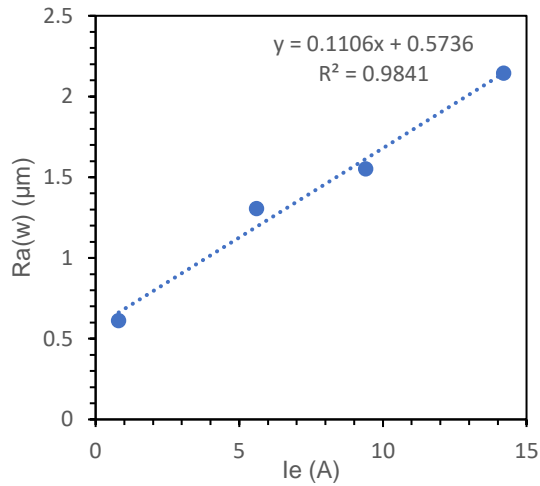
Figure 4-24 – Optimization experiment digitalized surfaces. (a) Workpiece machined surface and (b) Electrode machined surface. Note, scale global dimension equal to 0.25 mm.

The following table contains the process data responses resulted in this experiment.

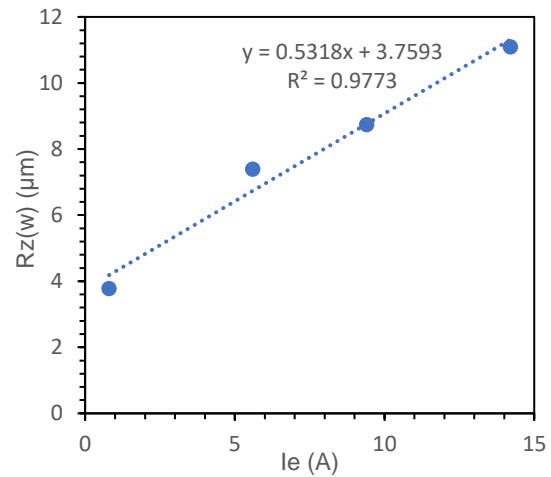
Table 18 - Process responses data for optimization experiment.

$Ra_W$ ( $\mu\text{m}$ )	$Rz_W$ ( $\mu\text{m}$ )	$Ra_{Ef}$ ( $\mu\text{m}$ )	$Rz_{Ef}$ ( $\mu\text{m}$ )	$T_{mach}$ (min)	MRR (g/min)	EWR (g/min)	WR
0.612	3.775	0.356	1.868	562.2	7.47E-05	1.42E-05	0.068

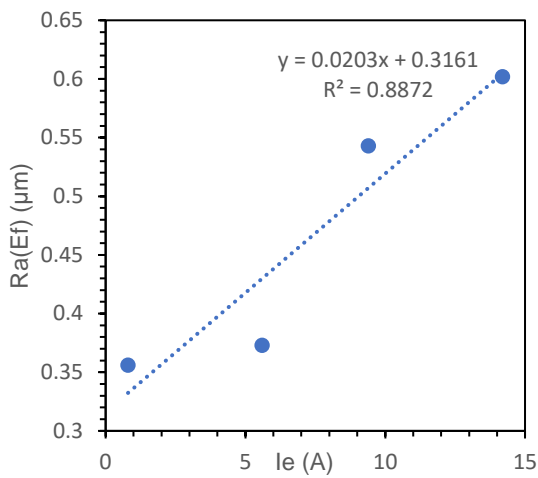
This result is plotted together with the previous data with the  $T_{on}$  series at  $1 \mu\text{s}$ , being presented in figure 4-25.



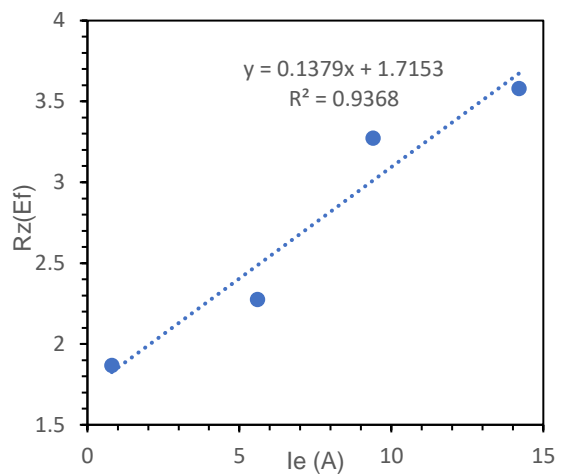
(a)



(b)



(c)



(d)

Figure 4-25 - Proof body surface roughness plot for open voltage of 80 V, pulse off time of 3  $\mu\text{s}$  and pulse on time of 1  $\mu\text{s}$ . (a)  $Ra_W$  relationship with electrical parameters; (b)  $Rz_W$  relationship with electrical parameters; (c)  $Ra_{Ef}$  relationship with electrical parameters; (d)  $Rz_{Ef}$  relationship with electrical parameters.

A machining strategy arises, in order to minimize surface roughness, as well as machining time, a program is created for machining a pocket with a depth of 0,2 mm. This machining program consists in different electrical signatures, starting with a high heat input, for a “rough” pass removing the larger amount of material, decreasing consecutively the energy per discharge until the last finishing pass. Avoiding taper-cut errors, electrode describes a linear orbit movement, increasing consecutively the step dimension until the last pass, having the first passes a safe side and safe depth distance, and in this way, previous machining craters are “erased” continuously in the moment electrical signatures change combined at different depths. As conclusion of electrical parameters results we denote that the smaller discharge energy leads to the smaller SR, with this, the values chosen for discharge current and pulse on time is respectively, 0,8 A and 1  $\mu\text{s}$ . Table 19 contains all data program.

Table 19 - Program data.

Pass	Depth (mm)	Side_Step (mm)	Ie (A)	Ton ( $\mu$ s)
1	0.153	0.053	14.2	5
2	0.16	0.06	11	5
3	0.173	0.073	9.4	5
4	0.177	0.077	5.6	3
5	0.188	0.088	4	3
6	0.191	0.091	3.2	3
7	0.192	0.092	2.4	1
8	0.193	0.093	1.4	1
9	0.195	0.095	0.8	1

This machining program led us to a surface roughness of 0.721  $\mu$ m, and reduced the machining time, and consequently we achieved a better combined value of SR, MRR that is around 0.0015 g/min. This was the best approach, since in a single electrical signature isn't allowable to have a high MRR and a low SR. Process Responses data obtained by this machining strategy are presented on the following table.

Table 20 - Process responses data for multiple electrical signatures.

$Ra_W$ ( $\mu$ m)	$Rz_W$ ( $\mu$ m)	$Ra_{Ef}$ ( $\mu$ m)	$Rz_{Ef}$ ( $\mu$ m)	$T_{mach}$ (min)	MRR (g/min)	EWR (g/min)	WR
0.721	4.305	0.545	3.01	19.8	0.00146341	0.00025231	0.052

The figures following presented, show the proof body aesthetics for the experiment performed with multiple electrical signatures.



(a)



(b)

Figure 4-26 - Proof body aesthetics for the multiple electrical signatures experiment. (a) Workpiece machined surface and (b) Electrode machined surface.

Even with this machining strategy, some black dots appear on the machined surfaces proof body. These are of significant less number than in the previous experiment with a single electrical signature, because its machining time was far lower.



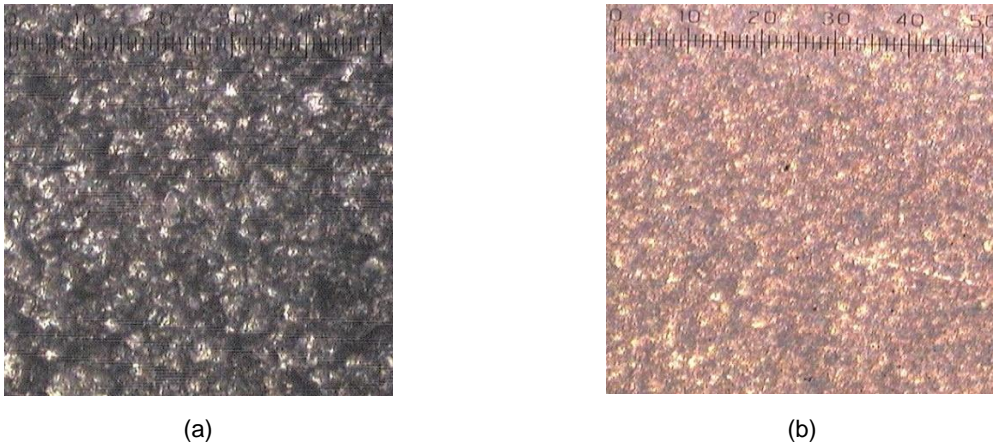


Figure 4-27 - Proof body microscopic view for the multiple electrical signature experiments. (a) Workpiece machined surface and (b) Electrode machined surface. Note, global scale dimension equal to 0.25 mm.

Summarily, this subchapter presents a method to achieve a fine surface finish together with a better material removal rate. It is also an empirical optimization, because by analysing electrical parameters influence experiments we concluded by graphical observation as well with Data Means and Signal to Noise Correlation function that the lower levels of discharge current and pulse on time lead to a better surface finish quality. Now comparing tables 18 and 20 data, we denote a general smaller increase in terms of SR, around  $0.1 \mu\text{m}$  in  $Ra_w$ , but main point of comparison is the reduced machining time from 9.5 hours to 20 minutes, that consequently increases MRR. EWR increases with this lower machining time, but WR is reduced by 0.016. Besides the greater number of black spots appearing on the workpiece for a single electrical signature, figure 4-28 (a), it presents more uniform craters dimension than figure 4-28 (b). Following table compares the microscopic view of the single electrical signature with the one with multiple signatures in a more amplified window on microscope.

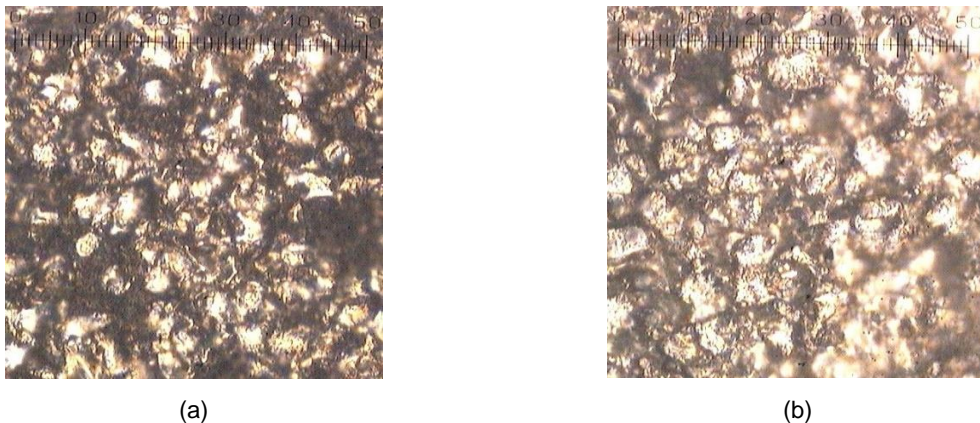


Figure 4-28 - Microscopic view of machined surfaces. (a) Workpiece machined surface for single electrical signature; (b) Workpiece machined surface for multiple electrical signatures. Note, global scale dimension equal to 0.1 mm.

## 5 Conclusions and future work

This aluminium alloy has shown to be of worse machinability than other typical material used in Electrical Discharge Machining. To justify this affirmation, we have the lower MRR and higher EWR, WR, and Ra. This was foreseen, once aluminium erosion index is higher than steel (as example), where even with a lower Melting Point, it has a high Specific Heat and Thermal Conductivity. These two properties induce in lower temperatures increase, and that is reflected on MRR, EWR and consequently in WR. It is important to refer that a lot of preliminary experiments were performed in order to find a suitable region of parameters to present experiments on electrical parameters experiments sub chapter. Optimum electrical parameters level combination was identified to be at lower discharge current and pulse on time, at 5.6 A and 1  $\mu$ s in terms of global SR and EWR. On the other hand, MRR is identified to be at the higher lower discharge current and pulse on time, at 14.2 A and 5  $\mu$ s. Mean level of discharge current and pulse on time at 5  $\mu$ s revealed optimum for WR. By empirical optimization, discharge current was reduced to 0.8 A achieving a Ra value of 0.612  $\mu$ m, where MRR dramatically decreased due to the increased machining time of 9.5 hours. Also, this experiment resulted on a poor aesthetics view with an ingrained black dot standard printed on both electrode and workpiece surfaces. Machining strategy with multiple electrical signatures above explained, proved itself useful decreasing machining time to 20 minutes and reducing significantly the number of black dots.

In terms of Electrode Roughness influence, levels of stability, increases and decreases were identified, a non-electrical parameter that was not found in any study on bibliography. It was decided to see if there was any influence because in theoretical articles there was always a reference that the inverted geometry is gradually printed in the workpiece [2]. There was a strict relation between Electrode and Workpiece Roughness, and it may be seen in figure 4-11. Three regions were identified, where at first roughness was steady, at a second stage where it presents an approximately linear growth and at last it tends to stabilize. Polished electrodes revealed to increase their roughness, with the increase of machining time, while the opposite occurred for rougher electrodes. Initial Electrode Roughness comprehended between 0.7 and 0.8  $\mu$ m present a constant evolution with no significant variation between Ra values while increasing machining time.

For future works, cylindrical shaped electrodes can be used as case study, where these can be obtained by lathe machining. Performing a facing operation with a controlled tool feed speed will lead to a more accurate electrode SR value. By varying tool feed speed other SR series can be achieved. Also, a more uniform surface can be obtained where SR will be radial distributed and of easier concentric measuring with a surface roughness measuring instrument.



# Bibliography

- [1] – Society of Manufacturing Engineers, 1996.  
<https://www.sme.org/WorkArea/DownloadAsset.aspx?id=63975>. Consulted on 12-03-2018
- [2] - Kunieda M., Lauwers B., Rajurkar KP, Schumacher B.M., Advancing EDM through fundamental insight into the process, Annals of the CIRP, (2005), 54, 599-622.
- [3] - Kumar S.; Singh R; Singh T.P; Sethi B.L.; “Surface modification by electrical discharge machining: A review”; Journal of Materials Processing Technology 209 (2009).
- [4] - Sunil Gaikwad, S.N. Teli, L.M. Gaikwad; “Optimization of EDM parameters on machining Ti6Al-4V with a core electrode using grey relational analysis” International Journal of Research in Aeronautical and Mechanical Engineering, Vol.2 Issue.12, December 2014. Pgs: 24-31
- [5] – Yihawjet Enterprises Co.,Ltd.  
[https://www.google.com/search?biw=1344&bih=657&tbm=isch&sa=1&ei=czo9W6DxEcyBgAbUgLaQDQ&q=moldmaster+yawjet&oq=moldmaster+yawjet&gs\\_l=img.3...0.0.0.218590.0.0.0.0.0.0.0.0...0...1c..64.img..0.0.0...0.yB0Y0R2vZBE](https://www.google.com/search?biw=1344&bih=657&tbm=isch&sa=1&ei=czo9W6DxEcyBgAbUgLaQDQ&q=moldmaster+yawjet&oq=moldmaster+yawjet&gs_l=img.3...0.0.0.218590.0.0.0.0.0.0.0.0...0...1c..64.img..0.0.0...0.yB0Y0R2vZBE). Consulted on 12-05-2018
- [6] - Liu K.; Lauwers B.; Reynaerts D.;” Process capabilities of Micro-EDM and its applications” International Journey of Advanced Manufacturing Technology (2010) 47:11–19
- [7] - Liu K.; Lauwers B.; Reynaerts D.; “Influence of pulse shape on EDM performance of  $Si_3N_4 - TiN$  ceramic composite” CIRP Annals – Manufacturing Technology – 58 (2009) 217-220
- [8] - Reynaerts D., Heeren P.-H., Brussel H. V., “Microstructuring of silicon by electro-discharge machining (EDM) - part I: theory “, Machine design Automation, Belgium, Sensors and Actuators A 60, 212-218, 1997.
- [9] - Mahendran S., Devarajan R., Nagarajan T., and Majdi A. “A Review of Micro-EDM”, (2010) Proceedings of the international multi conference of engineers and computer scientists.
- [10] - P. Balasubramanian; T. Senthilvelan; “Optimization of Machining Parameters in EDM process using Cast and Sintered Copper Electrodes”, (2014) 3rd International Conference on Materials Processing and Characterisation (ICMPC 2014), Procedia Materials Science 6 ( 2014 ) 1292 – 1302.
- [11] – Gostimirovic M., Kovac P., Sekulic M.and Skoric. “Influence of discharge energy on machining characteristics in EDM” Journal of Mechanical Science and Technology 26 (1) (2012) 173–179.
- [12] – Lee H. T. Hsu F.; Tai T.; ”Study of surface integrity using small area EDM process with a copper-tungsten electrode”, Materials Science and Engineering, 2004.
- [13] - Khan A.; “Role of Heat Transfer on Process Characteristics During Electrical Discharge Machining”, International Islamic University Malaysia,2011.

[14] - Kruth J. P.; Stevens L.; Froyen L.; Lauwers B.; "Study of the White Layer of a Surface Machined by Die-Sinking Electro-Discharge Machining", Annals of the CIRP Vol.44, 1995.

[15] – Kharola A.; "Analysis of Various Machining Parameters of Electrical Discharge Machining (EDM) on Hard Steels using Copper and Aluminium Electrodes", I.J. Engineering and Manufacturing, 2015, 1, 1-14

[16] – Laxman J; Kotakonda G. R;" Optimization of Electric Discharge Machining Process Parameters Using Taguchi Technique" International Journal of Advanced Mechanical Engineering. ISSN 2250-3234 Volume 4, Number 7 (2014), pp. 729-739.